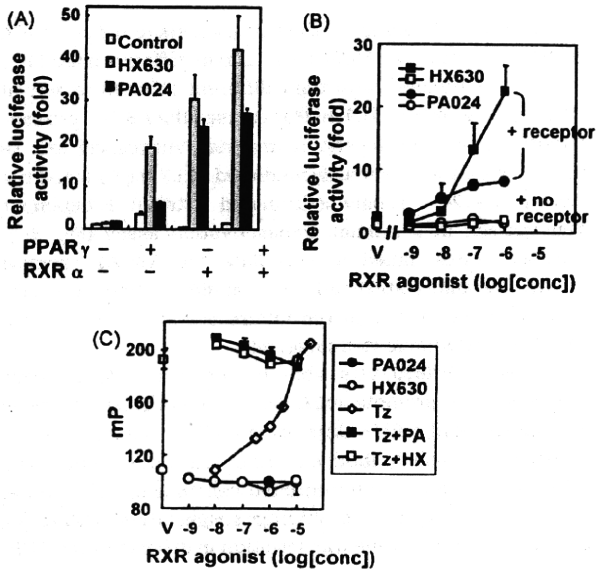


**Fig. 4 – PA024 and HX630 stimulate PPARγ/RXR transactivation. (A) RAW264 cells were transfected with a PPRE-tk-Luc reporter plasmid together with a phRL-TK internal control in the presence or absence of expression plasmids for human PPARγ and RXRα. The cells were treated with 100 nM PA024 or HX630 for 24 h before analysis. (B) Dose–response of RXR agonists for activation of a reporter gene by PPARγ/RXR. Cells were transfected with a PPRE-tk-Luc reporter plasmid in the absence (open symbols) or presence (closed symbols) of the PPARγ expression plasmid and treated with drugs for 24 h. Luciferase activity stimulated by PPARγ and endogenous RXR in the cell extract was determined, normalized, and expressed as fold induction relative to vehicle-treated cells without exogenous receptor expression. The values represent the average ± S.D. of three incubations. (C) RXR agonists do not affect binding of troglitazone to PPARγ. A fluorescent-tagged SRC-1 peptide (0.1 μM) was incubated with 1.5 μM PPARγ ligand binding domain in the presence of various concentrations of PA024 and HX630 in the presence or absence of 10 μM troglitazone (Tz). Ligand-induced association of coactivator peptide with the receptor was monitored by increases in millipolarization fluorescence units (mP).**

RXRα alone, the two agonists increased luciferase activity, indicating substantial activation of RXRα homodimer. However, when PPARγ alone was co-transfected, both agonists greatly enhanced transcription, suggesting that they have abilities to activate PPARγ/RXR heterodimer made from exogenous PPARγ and endogenous RXR. In this reporter assay system using exogenous PPARγ and endogenous RXR, HX630 activated PPARγ/RXR-dependent transcription more potently than PA024 at concentrations higher than 100 nM (Fig. 4B). To exclude the possibility that the HX630 and PA024 bind to PPARγ as a ligand, coactivator-association assay was performed. As shown in Fig. 4C, neither HX630 nor PA024 induced an interaction between fluorescence-labeled coactivator peptide and the PPARγ ligand binding domain *in vitro*, while the PPARγ agonist troglitazone strongly induced association. Furthermore, these RXR agonists did not affect the PPARγ-coactivator interaction elicited by 10 μM troglitazone. These findings indicate that the two RXR agonists were able to activate PPARγ/RXR.

### 3.4. *Possible stimulation of PPARγ-LXR-ABCA1 pathway by HX630*

LXRα gene is known to be a direct target of PPARγ/RXR, and stimulation of PPARγ has been shown to increase LXR-target gene expression by increasing LXRα expression [30]. We therefore examined the ability of HX630 to enhance LXR-target gene transcription by activating PPARγ/RXR. LXRE-driven luciferase assay was performed in RAW264 cells with or without co-transfection of PPARγ. As shown in Fig. 5A, HX630 augmented luciferase transcription in the presence but not in the absence or PPARγ. This effect was enhanced by increasing the amount of the PPARγ expression plasmid and the combination of HX630 and the LXR agonist 22(R)-hydroxycholesterol had an additive effect. The activity of ABCA1 promoter was also increased by HX630 when PPARγ was co-transfected (Fig. 5B)

The level of PPARγ mRNA was very low in undifferentiated THP-1 cells (not treated with PMA) but up-regulated during differentiation with PMA (Fig. 6). The levels of PPARγ-target gene CD36 and LXRα mRNA were unaffected by HX630 (100 nM) in undifferentiated cells but increased in PMA-differentiated cells (by 1.4- and 1.6-fold, respectively). In parallel with these changes, LXRα-target ABCG1 expression was unaffected by HX630 in undifferentiated THP-1 cells but increased in differentiated cells (by 3.9-fold). PA024 (100 nM) effectively raised ABCG1 and LXRα levels in undifferentiated

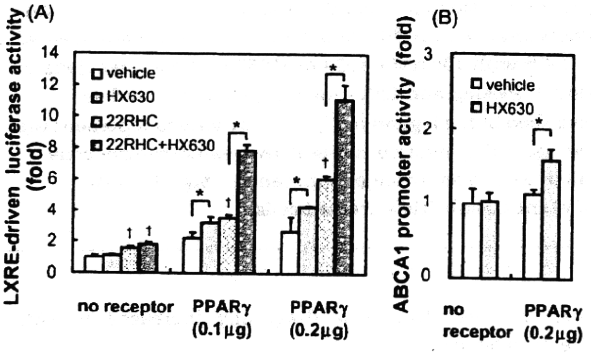


**Fig. 5 – HX630 activates LXRE-driven luciferase (A) or ABCA1 promoter (B) gene transcription upon co-expression of PPARγ. RAW264 cells were transfected with an LXREx4-tk-Luc or a pABCA1-Luc reporter plasmid and a phRL-TK internal control in the presence of 0–0.2 μg of PPARγ plasmid and treated for 24 with 100 nM HX630 in the presence or absence of 0.5 μg/ml 22(R)-hydroxycholesterol (22RHC). Luciferase activity in the cell extract was determined and normalized. The values represent the average ± S.D. of three experiments. Significantly different from respective control (*) or vehicle-treated cells (†).**

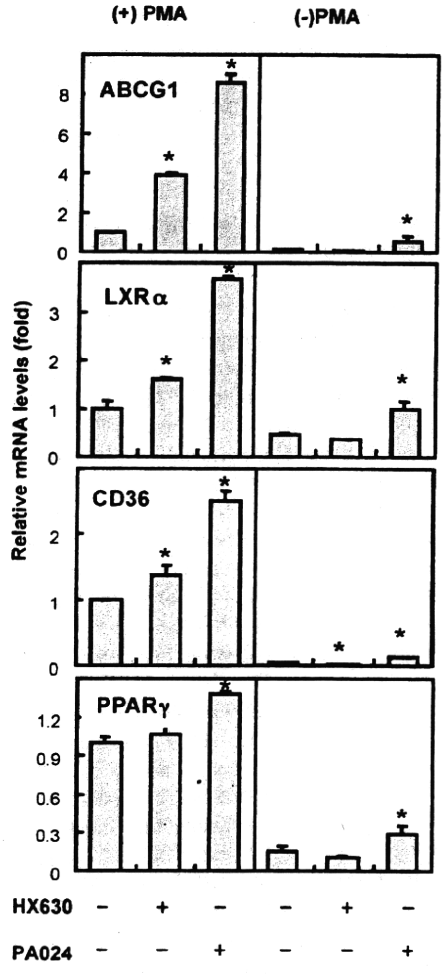


**Fig. 6 – PA024 and HX630 increase LXR- and PPARγ-target gene expressions in PMA-differentiated THP-1 cells. PMA-differentiated or undifferentiated THP-1 cells were treated for 24 h with 100 nM PA024 or HX630. The expressions of ABCG1, PPARγ, and LXRα mRNA were measured as described in the legend to Fig. 1B. The values represent the average ± S.D. relative to the PMA-treated control cells (taken as 1) from three experiments. * Significantly different from vehicle-treated cells.**

cells, and the effect was drastically increased in PMA-differentiated cells.

## 4. Discussion

In the present study, we found that RXR agonist PA024 efficiently enhanced ABCA1 mRNA expression in all cell lines tested and strongly promoted apoA-I-mediated cholesterol release (HDL generation) from PMA-differentiated THP-1 cells (Fig. 1B and C). However, HX630 was unable to raise the ABCA1 mRNA level in RAW264 cells (Fig. 1A) and undifferentiated THP-1 cells (Fig. 1B), but was active in differentiated THP-1 cells (Fig. 1B).

The different abilities of the two agonists to induce ABCA1 mRNA expression in RAW264 cells and undifferentiated THP-1 cells were paralleled with their different abilities to activate ABCA1 promoter (Fig. 2). PA024 increased the ABCA1 promoter activity in an LXRE-dependent manner, suggesting that the effect of PA024 was primarily mediated by LXR/RXR activation. Indeed, PA024 strongly stimulated LXRα/RXR-dependent transcription in a cellular transactivation assay (Fig. 3). In contrast, HX630 failed to stimulate the ABCA1 promoter activity. Because HX630 had no capability to directly activate LXR/RXR, suggesting that the failure of ABCA1 induction by HX630 is attributable to this defect.

However, HX630 was able to increase ABCA1 mRNA expression and promote apoA-I-mediated cholesterol release (HDL generation) in PMA-differentiated THP-1 cells (Fig. 1B and C). HX630 was able to induce another LXR-target gene ABCG1 mRNA expression in differentiated cells but not in undifferentiated cells (Fig. 6). These findings suggest that HX630 might increase LXR-target gene transcription in differentiated THP-1 cells.

The LXRα gene is known to be a direct target of PPARγ, and stimulation of PPARγ by agonists has been shown to increase ABCA1 expression by raising LXRα level [30]. We showed that both HX630 and PA024 were able to activate PPARγ/RXR in a cellular transactivation assay (Fig. 4). Furthermore, if PPARγ-expression plasmid was co-transfected into RAW264 cells, HX630 was able to stimulate an LXRE-dependent reporter gene transcription and the ABCA1 promoter activity, as well (Fig. 5). These findings suggest the ability of HX630 to stimulate the PPARγ-LXR-ABCA1 pathway. The level of PPARγ mRNA was greatly induced by differentiation of THP-1 cells with PMA (Fig. 6). In addition, the differentiation augmented HX630-mediated expression of LXR-target ABCA1 and ABCG1 and PPARγ-target LXRα and CD36. Both endogenous PPARγ activity (Fig. 4A and B) and HX630-induced ABCA1 expression (Fig. 1A) were undetectable in RAW264 cells. These findings indicate a close correlation between the ability of HX630 to enhance LXR-target gene expression and the cellular PPARγ mRNA level. The activation of PPARγ/RXR by HX630 primary may elevate LXRα and thereby enhances ABCA1 expression in PMA-differentiated THP-1 cells. Possibility remains that HX630 stimulates LXR/RXR in this cell model. However, we were unable to investigate this possibility due to very low efficiency in DNA transfection in PMA-differentiated cells. Another possibility is that activation of RXR heterodimer(s) other than PPARγ/RXR may also be responsible for the HX630-mediated ABCA1 expression in this cell line. A study has shown that RAR activators increase ABCA1 expression in mouse peripheral macrophages, and that RAR/RXR stimulated the ABCA1 promoter activity via the same DR4 element as LXR/RXR [31]. However, when PMA-differentiated THP-1 cells were treated with RAR agonist AM80 [21], the ABCA1 mRNA level was unchanged (data not shown), suggesting that the RAR/RXR-mediated promoter activation may not make a large contribution to ABCA1 expression in this cell line.

Inductions of ABCA1 and HDL generation by PA024 and HX630 were accompanied by a decrease in the cellular cholesterol level (Fig. 1C). In particular, our findings show the effectiveness of direct activation of LXR/RXR by PA024 (Fig. 3). Although LXR/RXR is known to be permissive in terms

of RXR agonist activation [16,17], HX630 was unable to activate LXR/RXR (Fig. 3). Administration of RXR agonists to mice leads to increases in HDL cholesterol levels [20]. RXR modulators are promising therapeutic strategies [32]. However, increases in serum triglyceride due to RXR agonists are postulated to occur via activation of LXR/RXR, leading to enhanced lipogenesis in response to induction of hepatic SREBP-1c expression [33]. Heterodimer-selective RXR agonists without the ability to directly activate LXR/RXR, may be a promising target for the development of drugs without adverse effects. Synthetic RXR agonists that retain the ability to activate PPARγ/RXR, but have less effect on LXR/RXR and RAR/RXR, have been reported, and pharmacological advantages of these heterodimer-selective RXR agonists as anti-diabetes agents have been demonstrated [34]. The molecular basis of such heterodimer selectivity has not fully been clarified. The mechanism underlying HX630 heterodimer selectivity awaits further investigation.

## Acknowledgments

This work was supported in part by a grant from the Japan Health Sciences Foundation, a grant (MF-16) from the Organization for Pharmaceutical Safety and Research, and Grant-in-Aid for Scientific Research 20590116 from Japan Society for the Promotion of Science.

## REFERENCES

[1] Yokoyama S. Assembly of high-density lipoprotein. Arterioscler Thromb Vasc Biol 2006;26:20–7.
[2] Bodzioch M, Orso E, Klucken J, Langmann T, Bottcher A, Diederich W, et al. The gene encoding ATP-binding cassette transporter 1 is mutated in Tangier disease. Nat Genet 1999;22:347–51.
[3] Brooks-Wilson A, Marcil M, Clee SM, Zhang LH, Roomp K, van Dam M, et al. Mutations in ABC1 in Tangier disease and familial high-density lipoprotein deficiency. Nat Genet 1999;22:336–45.
[4] Rust S, Rosier M, Funke H, Real J, Amoura Z, Piette JC, et al. Tangier disease is caused by mutations in the gene encoding ATP-binding cassette transporter 1. Nat Genet 1999;22:352–5.
[5] Singaraja RR, Bocher V, James ER, Clee SM, Zhang LH, Leavitt BR, et al. Human ABCA1 BAC transgenic mice show increased high density lipoprotein cholesterol and apoAI-dependent efflux stimulated by an internal promoter containing liver X receptor response elements in intron 1. J Biol Chem 2001;276:33969–7.
[6] Vaisman BL, Lambert G, Amar M, Joyce C, Ito T, Shamburek RD, et al. ABCA1 overexpression leads to hyperalphalipoproteinemia and increased biliary cholesterol excretion in transgenic mice. J Clin Invest 2001;108:303–9.
[7] Joyce CW, Amar MJ, Lambert G, Vaisman BL, Paigen B, Najib-Fruchart J, et al. The ATP binding cassette transporter A1 (ABCA1) modulates the development of aortic atherosclerosis in C57BL/6 and apoE-knockout mice. Proc Natl Acad Sci USA 2002;99:407–12.
[8] Singaraja RR, Fievet C, Castro G, James ER, Hennuyer N, Clee SM, et al. Increased ABCA1 activity protects against atherosclerosis. J Clin Invest 2002;110:35–42.
[9] Gordon T, Castelli WP, Hjortland MC, Kannel WB, Dawber TR. High density lipoprotein as a protective factor against coronary heart disease. The Framingham study. Am J Med 1977;62:707–14.
[10] Fielding CJ, Fielding PE. Molecular physiology of reverse cholesterol transport. J Lipid Res 1995;36:211–28.
[11] Costet P, Luo Y, Wang N, Tall AR. Sterol-dependent transactivation of the ABC1 promoter by the liver X receptor/retinoid X receptor. J Biol Chem 2000;275:28240–5.
[12] Langmann T, Klucken J, Reil M, Liebisch G, Luciani MF, Chimini G, et al. Molecular cloning of the human ATP-binding cassette transporter 1 (hABC1): evidence for sterol-dependent regulation in macrophages. Biochem Biophys Res Commun 1999;257:29–33.
[13] Schwartz K, Lawn RM, Wade DP. ABC1 gene expression and apoA-I-mediated cholesterol efflux are regulated by LXR. Biochem Biophys Res Commun 2000;274:794–802.
[14] Venkateswaran A, Laffitte BA, Joseph SB, Mak PA, Wilpitz DC, Edwards PA, et al. Control of cellular cholesterol efflux by the nuclear oxysterol receptor LXR alpha. Proc Natl Acad Sci USA 2000;97:12097–102.
[15] Chinetti G, Lestavel S, Bocher V, Remaley AT, Neve B, Torra IP, et al. PPAR-alpha and PPAR-gamma activators induce cholesterol removal from human macrophage foam cells through stimulation of the ABCA1 pathway. Nat Med 2001;7:53–8.
[16] Chawla A, Repa JJ, Evans RM, Mangelsdorf DJ. Nuclear receptors and lipid physiology: opening the X-files. Science 2001;294:1866–70.
[17] Mangelsdorf DJ, Evans RM. The RXR heterodimers and orphan receptors. Cell 1995;83:841–50.
[18] Mukherjee R, Davies PJ, Crombie DL, Bischoff ED, Cesario RM, Jow L, et al. Sensitization of diabetic and obese mice to insulin by retinoid X receptor agonists. Nature 1997;386:407–10.
[19] Claudel T, Leibowitz MD, Fievet C, Tailleux A, Wagner B, Repa JJ, et al. Reduction of atherosclerosis in apolipoprotein E knockout mice by activation of the retinoid X receptor. Proc Natl Acad Sci USA 2001;98:2610–5.
[20] Repa JJ, Turley SD, Lobaccaro JA, Medina J, Li L, Lustig K, et al. Regulation of absorption and ABC1-mediated efflux of cholesterol by RXR heterodimers. Science 2000;289:1524–9.
[21] Kagechika H, Shudo K. Synthetic retinoids: recent developments concerning structure and clinical utility. J Med Chem 2005;48:5875–83.
[22] Ohta K, Kawachi E, Inoue N, Fukasawa H, Hashimoto Y, Itai A, et al. Retinoidal pyrimidinecarboxylic acids. Unexpected diaza-substituent effects in retinobenzoic acids. Chem Pharm Bull (Tokyo) 2000;48:1504–13.
[23] Umemiya H, Fukasawa H, Ebisawa M, Eyrolles L, Kawachi E, Eisenmann G, et al. Regulation of retinoidal actions by diazepinylbenzoic acids. Retinoid synergists which activate the RXR–RAR heterodimers. J Med Chem 1997;40:4222–34.
[24] Suzuki S, Nishimaki-Mogami T, Tamehiro N, Inoue K, Arakawa R, Abe-Dohmae S, et al. Verapamil increases the apolipoprotein-mediated release of cellular cholesterol by induction of ABCA1 expression via Liver X receptor-independent mechanism. Arterioscler Thromb Vasc Biol 2004;24:519–25.
[25] Fu X, Menke JG, Chen Y, Zhou G, MacNaul KL, Wright SD, et al. 27-hydroxycholesterol is an endogenous ligand for liver X receptor in cholesterol-loaded cells. J Biol Chem 2001;276:38378–87.
[26] Tamehiro N, Shigemoto-Mogami Y, Kakeya T, Okuhira K, Suzuki K, Sato R, et al. Sterol regulatory element-binding protein-2- and liver X receptor-driven dual promoter regulation of hepatic ABC transporter A1 gene expression: mechanism underlying the unique response to cellular cholesterol status. J Biol Chem 2007;282:21090–9.

[27] Nishimaki-Mogami T, Une M, Fujino T, Sato Y, Tamehiro N, Kawahara Y, et al. Identification of intermediates in the bile acid synthetic pathway as ligands for the farnesoid X receptor. J Lipid Res 2004;45: 1538–45.
[28] Abe-Dohmae S, Suzuki S, Wada Y, Aburatani H, Vance DE, Yokoyama S. Characterization of apolipoprotein-mediated HDL generation induced by cAMP in a murine macrophage cell line. Biochemistry 2000;39:11092–9.
[29] Umemiya H, Kagechika H, Fukasawa H, Kawachi E, Ebisawa M, Hashimoto Y, et al. Action mechanism of retinoid-synergistic dibenzodiazepines. Biochem Biophys Res Commun 1997;233:121–5.
[30] Chawla A, Boisvert WA, Lee CH, Laffitte BA, Barak Y, Joseph SB, et al. A PPAR gamma-LXR-ABCA1 pathway in macrophages is involved in cholesterol efflux and atherogenesis. Mol Cell 2001;7:161–71.
[31] Costet P, Lalanne F, Gerbod-Giannone MC, Molina JR, Fu X, Lund EG, et al. Retinoic acid receptor-mediated induction of ABCA1 in macrophages. Mol Cell Biol 2003;23:7756–66.
[32] Altucci L, Leibowitz MD, Ogilvie KM, de Lera AR, Gronemeyer H. RAR and RXR modulation in cancer and metabolic disease. Nat Rev Drug Discov 2007;6:793–810.
[33] Schultz JR, Tu H, Luk A, Repa JJ, Medina JC, Li L, et al. Role of LXRs in control of lipogenesis. Genes Dev 2000;14:2831–8.
[34] Michellys PY, Ardecky RJ, Chen JH, Crombie DL, Etgen GJ, Faul MM, et al. Novel (2E,4E,6Z)-7-(2-alkoxy-3,5-dialkylbenzene)-3-methylocta-2,4,6-trienoic acid retinoid X receptor modulators are active in models of type 2 diabetes. J Med Chem 2003;46:2683–96.

# Glycosylation Analysis of IgLON Family Proteins in Rat Brain by Liquid Chromatography and Multiple-Stage Mass Spectrometry

**Satsuki Itoh, Akiko Hachisuka, Nana Kawasaki, Noritaka Hashii, Reiko Teshima, Takao Hayakawa, Toru Kawanishi, and Teruhide Yamaguchi**

Division of Biological Chemistry and Biologicals, National Institute of Health Sciences, 1-18-1, Kamiyoga, Setagaya-ku, Tokyo 158-8501, Japan, Core Research for Evolutional Science and Technology of Japan Science and Technology Agency, Kawaguchi Center Building, 4-1-8 Hon-cho, Kawaguchi, Saitama 332-0012, Japan, and Pharmaceutical Research and Technology Institute, Kinki University, 3-4-1 Kowakae, Higashi-Osaka 577-8502, Japan

Biochemistry®

Reprinted from
Volume 47, Number 38, Pages 10132–10154

# Glycosylation Analysis of IgLON Family Proteins in Rat Brain by Liquid Chromatography and Multiple-Stage Mass Spectrometry†

Satsuki Itoh,‡ Akiko Hachisuka,‡ Nana Kawasaki,*,‡,§ Noritaka Hashii,‡ Reiko Teshima,‡ Takao Hayakawa,|| Toru Kawanishi,‡ and Teruhide Yamaguchi‡

*Division of Biological Chemistry and Biologicals, National Institute of Health Sciences, 1-18-1, Kamiyoga, Setagaya-ku, Tokyo 158-8501, Japan, Core Research for Evolutional Science and Technology of Japan Science and Technology Agency, Kawaguchi Center Building, 4-1-8 Hon-cho, Kawaguchi, Saitama 332-0012, Japan, and Pharmaceutical Research and Technology Institute, Kinki University, 3-4-1 Kowakae, Higashi-Osaka 577-8502, Japan*

*Received May 23, 2008; Revised Manuscript Received July 17, 2008*

ABSTRACT: IgLON family proteins, including limbic-associated membrane protein (LAMP), opioid-binding cell adhesion molecule (OBCAM), neurotrimin, and Kilon, are immunoglobulin (Ig) superfamily cell adhesion molecules. These molecules are composed of three Ig domains and a glycosylphosphatidylinositol (GPI) anchor and contain six or seven potential N-glycosylation sites. Although their glycosylations are supposed to be associated with the development of the central nervous system like other Ig superfamily proteins, they are still unknown because of difficulty in isolating individual proteins with a high degree of homology in performing carbohydrate analysis. In this study, we conducted simultaneous site-specific glycosylation analysis of rat brain IgLON proteins by liquid chromatography and multiple-stage mass spectrometry (LC−$MS^n$). The rat brain GPI-linked proteins were enriched and separated by sodium dodecyl sulfate−polyacrylamide gel electrophoresis. The four proteins were extracted from the gel, and subjected to LC−$MS^n$ after proteinase digestions. A set of glycopeptide MS data, including the mass spectrum, the mass spectrum in the selected ion monitoring mode, and the product ion spectra, was selected from all data based on carbohydrate-related ions in the MS/MS spectrum. The peptide portion and the carbohydrate structure were identified on the basis of peptide-related ion and carbohydrate-related ions, and the accurate mass. The site-specific glycosylations of four proteins were elucidated as follows. *N*-Glycans near the N-terminal were disialic acid-conjugated complex- and hybrid-type oligosaccharides. The first Ig domains were occupied by Man-5-9. Diverse oligosaccharides, including Lewis a/x-modified glycans, a brain-specific glycan known as BA-2, and Man-5, were found to be attached to the third Ig domain. Three common structures of glycans were found in the GPI moiety of LAMP, OBCAM, and neurotrimin.

Cell adhesion molecules on cell surfaces are involved in several biological events, such as cell−cell interaction, signaling, and cellular traffic. In the central nervous system, cell adhesion molecules are associated with the differentiation and migration of neurons, and neurite outgrowth. The immunoglobulin (Ig) superfamily, which contains one or more Ig-like domains, is known as one of the cell adhesion molecule families in the central nervous system (*1*). The Ig superfamily includes various proteins, such as P0, Thy-1, myelin-associated glycoprotein (MAG), neural cell adhesion molecule (NCAM), L1, contactin, and IgLON family proteins. Glycosylation of the Ig superfamily proteins is known to be involved in cell−cell interactions (*2*−*4*). Polysialylated glycans in the fifth domain of NCAM are thought to inhibit the interaction of NCAM with other molecules and to promote neural plasticity through a repulsive interaction (*5, 6*). The HNK-1 epitope in the third and fifth domains of NCAM is known to mediate molecular recognition in the nervous system (*7*).

The IgLON superfamily includes the limbic-associated membrane protein (LAMP),[1] the opioid-binding cell adhesion molecule (OBCAM), neurotrimin, and Kilon (*8*−*14*), and

† This work was supported in part by a Grant-in-Aid from the Ministry of Health and Labor and Welfare, and Core Research for Evolutional Science and Technology Program (CREST) of the Japan Science and Technology Agency (JST).

* To whom correspondence should be addressed: Division of Biological Chemistry and Biologicals, National Institute of Health Sciences, 1-18-1, Kamiyoga, Setagaya-ku, Tokyo 158-8501, Japan. Telephone: +81-3-3700-9074. Fax: +81-3-3707-6950. E-mail: nana@nihs.go.jp.

‡ National Institute of Health Sciences.

§ Core Research for Evolutional Science and Technology of Japan Science and Technology Agency.

|| Kinki University.

[1] Abbreviations: LC, liquid chromatography; MS, mass spectrometry; $MS^n$, multiple-stage mass spectrometry; LAMP, limbic-associated membrane protein; OBCAM, opioid-binding cell adhesion molecule; GlcNAc, *N*-acetylglucosamine; GPI, glycosylphosphatidylinositol; PI-PLC, phosphatidylinositol-specific phospholipase C; PNGase F, peptide *N*-glycosidase F; IT-MS, ion trap mass spectrometer; FT ICR-MS, Fourier transform ion cyclotron resonance mass spectrometer; GCC, graphitized carbon column; TIC, total ion chromatogram; CID, collision-induced dissociation; SIM, selected ion monitoring; dHex, deoxyhexose; Hex, hexose; HexNAc, *N*-acetylhexosamine; Fuc, fucose; Man, mannose; Gal, galactose; GlcNAc, *N*-acetylglucosamine; GlcN, glucosamine; NeuAc, *N*-acetylneuraminic acid; $EtNH_2$, ethanolamine; Ino, inositol; BA-2, brain-specific sugar chain, GlcNAcβ1−2Manα1−6(GlcNAcβ1−4)(GlcNAcβ1−2Manα1−3)Manβ1−4GlcNAcβ1−4(Fucα1−6)GlcNAc; SDS−PAGE, sodium dodecyl sulfate−polyacrylamide gel electrophoresis.

10.1021/bi8009778 CCC: $40.75 
Published on Web 08/26/2008

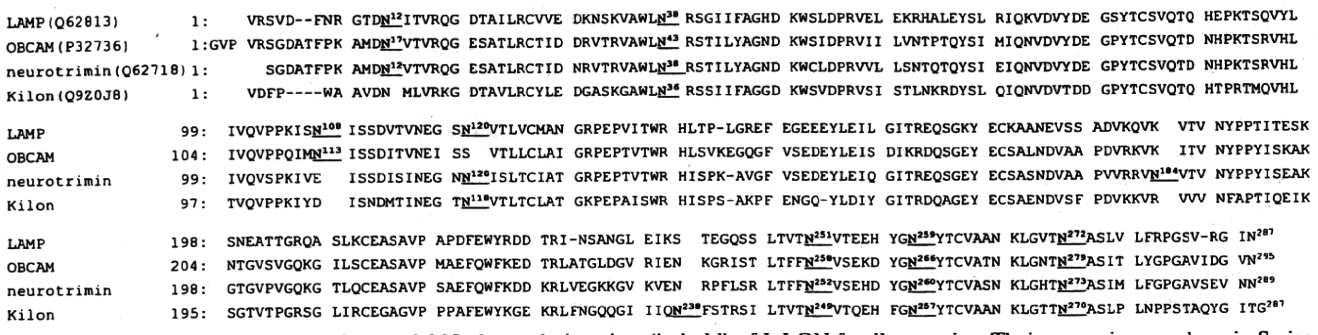


FIGURE 1: Amino acid sequence and potential N-glycosylation sites (in bold) of IgLON family proteins. Their accession numbers in Swiss-prot database are shown in parentheses after their names. The C-terminal amino acids in the proteins are predicted GPI attachment sites.

these proteins are distributed differently in the central nervous system during the development of neurons in a brain (*11*, *13*−*18*). The IgLON family proteins consist of three Ig domains, the third of which is attached to a glycosylphosphatidylinositol (GPI) anchor. Each of the IgLON family proteins includes six or seven consensus N-glycosylation sites (Figure 1), and the glycosylation is presumed to play essential roles in the neural circuit formation like other Ig superfamily proteins (*2*−*4*). However, since the high degree of homology of their amino acid sequences makes it difficult to isolate the individual proteins of this family to perform carbohydrate analysis, their glycosylation features are still unknown with the exception of a linkage of *N*-glycans in OBCAM and Kilon and of high mannose-type and hybrid-type oligosaccharides in LAMP (*9*, *18*, *19*).

Recently, liquid chromatography and mass spectrometry (LC−MS) and liquid chromatography and multiple-stage mass spectrometry (LC−MS$^n$) have been widely applied to the site-specific glycosylation analysis of a glycoprotein (*20*−*24*). Generally, a tryptic digest of an isolated glycoprotein is separated with a reversed-phase or normal-phase column, and the separated glycopeptides are directly subjected to MS and MS$^n$ (*25*−*27*). The site-specific glycosylation is deduced from the mass spectra of the glycopeptides, and the sequences of both the peptide and carbohydrate portions are deduced from the fragment ions in the MS$^n$ spectra. Using this technique, we previously performed a site-specific glycosylation analysis of rat brain Thy-1, which contains three N-glycosylation sites and a GPI anchor (*28*). GPI-anchored proteins enriched via phase partitioning with Triton X-114 and PIPLC digestion were separated by SDS−PAGE, and the Thy-1 protein extracted from the gel was digested with trypsin or endoproteinase Asp-N. The Thy-1 glycopeptides were separated and analyzed by using a liquid chromatography and ion trap mass spectrometer (IT-MS) equipped with a C18 column. The peptide portions of glycopeptides were identified on the basis of the *m*/*z* values of the peptide-related ions and the b- and y-ions that arose from the peptide backbone. The carbohydrate structures at each glycosylation site and in the GPI moiety were successfully determined from fragment ions in the MS/MS spectra. This result suggests that LC−MS$^n$ can be effectively utilized for site-specific glycosylation analysis of each glycoprotein in the mixture of several glycoproteins simultaneously.

In this study, we conducted site-specific glycosylation analyses of rat LAMP, OBCAM, neurotrimin, and Kilon using LC−MS$^n$. The GPI-linked proteins in the rat brains were separated by SDS−PAGE, and the IgLON family proteins were extracted from a gel band (45−70 kDa). The mixture of proteins was digested with proteinases, and the site-specific glycosylation analysis of the four proteins was performed by using an ion trap-Fourier transform ion cyclotron resonance mass spectrometer (IT-MS-FT ICR-MS), which is capable of acquiring the accurate mass as well as the MS$^n$ spectra. We successfully elucidated the site-specific glycosylation and the structure of the GPI moieties of LAMP, OBCAM, neurotrimin, and Kilon. This is the first report of the simultaneous site-specific glycosylation analysis of four similar glycoproteins.

## EXPERIMENTAL PROCEDURES

*Materials.* The rat brains (Wister, male, 3 weeks old) were purchased from Nippon SLC (Hamamatsu, Japan). Phosphatidylinositol-specific phospholipase C (PIPLC) from *Bacillus cereus* was obtained from Molecular Probes (Eugene, OR). Trypsin-Gold was purchased from Promega (Madison, WI). PNGase F and endoproteinase Glu-C were purchased from Roche Diagnostics (Mannheim, Germany). SimplyBlue SafeStain was obtained from Invitrogen (Carlsbad, CA). All other chemicals were of the highest available purity.

*SDS−PAGE of Enriched Lipid-Free GPI-Linked Proteins.* Lipid-free GPI-linked proteins were enriched from rat brain as reported previously (*28*, *29*). Briefly, the homogenate of two rat brains (total wet weight of 1.4 g) was defatted and solubilized with 2% Triton X-114 at 4 °C overnight (*29*, *30*). After centrifugation, the supernatant was subjected to Triton X-114 phase partitioning at 37 °C. Cold acetone was added to the detergent phase containing solubilized membrane proteins, and the resulting precipitate was digested with PIPLC. After the PIPLC digest mixture had been subjected to Triton X-114 phase partitioning, lipid-free GPI-linked proteins in the aqueous phase were precipitated via addition of cold acetone. These proteins were separated by SDS−PAGE (12.5%) (brain wet weight of 50 mg/lane) after carboxyamidomethylation (*31*) and detected after being stained with Coomassie Brilliant Blue G-250 using SimplyBlue SafeStain.

*Protein Identification.* Gel-separated proteins were extracted after in-gel trypsin digestion as previously reported (*32*) and subjected to LC−MS/MS with a Paradigm MS4 HPLC system (Michrom BioResources, Inc., Auburn, CA) consisting of pump A with 0.1% formic acid and 2% acetonitrile and pump B with 0.1% formic acid and 90% acetonitrile. Peptides were separated with a Magic C18 column (50 mm × 0.2 mm, 3 μm; Michrom BioResources Inc.) with a linear gradient from 5 to 65% of pump B over

20 min at a flow rate of 3 μL/min. Mass spectra were recorded with a Finnigan LTQ system (Thermo Fisher Scientific, Waltham, MA) using sequential scan events: MS (*m/z* 450−2000) followed by data-dependent MS/MS on the IT-MS for the most intense ions in positive ion mode. For protein identification, all obtained product ions were subjected to a computer database search analysis with the TurboSEQUEST search engine (Thermo Fisher Scientific) using the Swiss-Prot database and search parameters: a static modification of carboxyamidomethylation (57 Da) at Cys and trypsin for digestion.

*Extraction and Proteinase Digestion of the 45−70 kDa Proteins Separated by SDS−PAGE.* The gel-separated proteins were extracted as previously reported (*28*). The proteins were extracted with 20 mM Tris-HCl containing 1% SDS by being shaken vigorously overnight after the gel had been broken down into small bits. The extract was filtered with Ultrafree-MC (0.22 μm; Millipore, Bedford, MA), and the proteins were precipitated via addition of cold acetone. The resulting precipitate was digested with endoproteinase Glu-C (3.75 μg) in 30 μL of 0.1 M ammonium acetate (pH 8.0) at 37 °C for 4 days, followed by incubation with additional trypsin (1 μg) at 37 °C overnight.

*LC−MS$^n$.* Proteolytic peptides were separated by reversed-phase columns, Magic C30 and C18 (50 mm × 0.1 mm, 3 μm; Michrom BioResources), and a graphitized carbon column (GCC), Hypercarb 5 μ (150 mm × 0.2 mm; Thermo Fisher Scientific), with a Paradigm MS4 HPLC system consisting of pump A with 0.1% formic acid and 2% acetonitrile and pump B with 0.1% formic acid and 90% acetonitrile. For analysis of glycopeptides, separation was performed with a linear gradient from 5 to 50% pump B over 100 min followed by a 50 to 95% B gradient over 10 min and 95% B over 10 min at a flow rate of 0.5 μL/min, and mass spectra were recorded with a Finnigan LTQ-FT system (Thermo Fisher Scientific) using sequential scan events: MS (*m/z* 1000−2000 or 700−2000) with the IT-MS followed by MS with the IT-MS-FT ICR-MS in selected ion monitoring (SIM) mode and data-dependent MS$^n$ with the IT-MS for the most intense ions. The LC−MS$^n$ runs were performed with a C30 column and scan range of *m/z* 1000−2000 (condition A), twice, with a C30 column and scan range of *m/z* 700−2000 (condition B), once, and with a C18 column and scan range of *m/z* 1000−2000 (condition C), once. For analysis of GPI-linked peptides, separation was performed with a linear gradient from 5 to 60% pump B over 100 min at a flow rate of 2 μL/min for a GCC, and mass spectra were recorded with a Finnigan LTQ system using sequential scans: a single mass scan (*m/z* 700−2000) with the IT-MS followed by data-dependent MS$^n$ scans with the IT-MS for the most intense ions, twice. LC−MS$^n$ was performed using a capillary voltage of 1.8 kV and a capillary temperature of 200 °C.

## RESULTS

*Preparation of Lipid-Free IgLON Glycopeptides.* Figure 2 illustrates the experimental procedure for the glycosylation analysis of IgLON family proteins. Lipid-free GPI-linked proteins in a rat brain tissue sample were enriched via phase partitioning with Triton X-114 and PIPLC digestion. The enriched proteins were separated by SDS−PAGE and stained

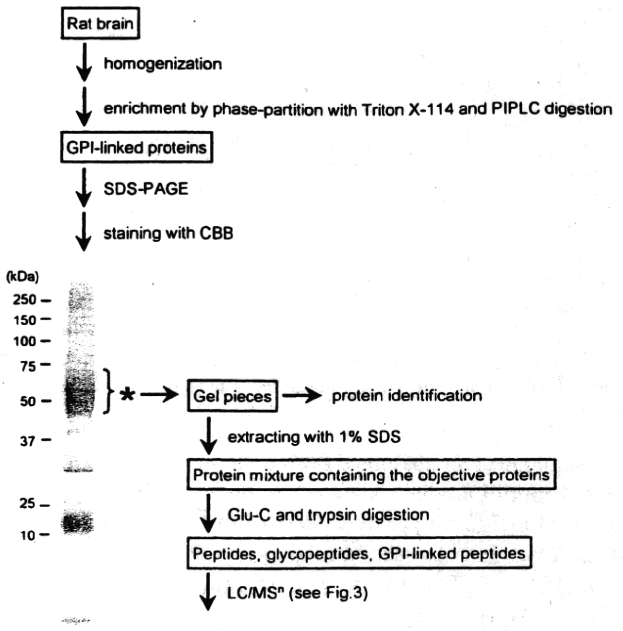


FIGURE 2: Experimental procedure for site-specific glycosylation analysis of IgLON family proteins and SDS−PAGE (12.5%) of lipid-free GPI-linked proteins which were enriched from rat brain. The asterisk indicates the gel band containing IgLON family proteins.

with Coomassie Brilliant Blue. The presence of LAMP, OBCAM, neurotrimin, and Kilon in the gel band at 45−70 kDa was confirmed by in-gel trypsin digestion followed by LC−MS/MS. The IgLON proteins were extracted with other comigrated proteins from 45−70 kDa bands in other lanes by being shaken in 1% SDS. After SDS had been removed, the mixture of proteins was digested with endoproteinase Glu-C and trypsin. Most of the resulting glycopeptides contained only a single N-glycosylation site, with the exception of LGTTN$^{270}$ASLPLNPPSTAQYGITG$^{287}$ in Kilon, which included a predicted GPI attachment site at Gly287 in addition to a potential N-glycosylation site at Asn270 (Figure 1). The glycopeptides from IgLON family proteins was separated by using three different columns: a reversed-phase column, a C30 and a C18 column for hydrophobic glycopeptides, and a GCC for hydrophilic glycopeptides, including GPI-linked peptides.

*Glycosylation Analysis of LAMP.* LC−MS analysis was performed via MS on the IT-MS and data-dependent MS in SIM mode on the FT ICR-MS, and data-dependent MS/MS and MS/MS/MS were performed on the IT-MS in the positive ion mode (Figure 3). After MS data acquisition, the MS/MS spectrum (scan *n*) of a glycopeptide was selected manually from all MS data on the basis of the existence of carbohydrate distinctive fragments, such as $Hex_1HexNAc_1^+$ (*m/z* 366) and $Hex_1HexNAc_1NeuAc^+$ (*m/z* 657). Then a set of the glycopeptide's MS data consisting of the mass spectrum (scan $n-2$), the mass spectrum in SIM on the FT ICR-MS (scan $n-1$), the MS/MS spectrum (scan *n*), and the MS/MS/MS spectrum (scan $n+1$) was selected from all the MS data (step 1). The carbohydrate structure was deduced from the fragment ions appearing in the MS/MS spectrum (scan *n*), and the peptide portion was estimated from the peptide-related ions (step 2). The sequences of some peptides were confirmed by the b- and y-ions that arose from $Y_1$ ([peptide + HexNAc + H]$^+$) in MS/MS/MS (scan $n+$

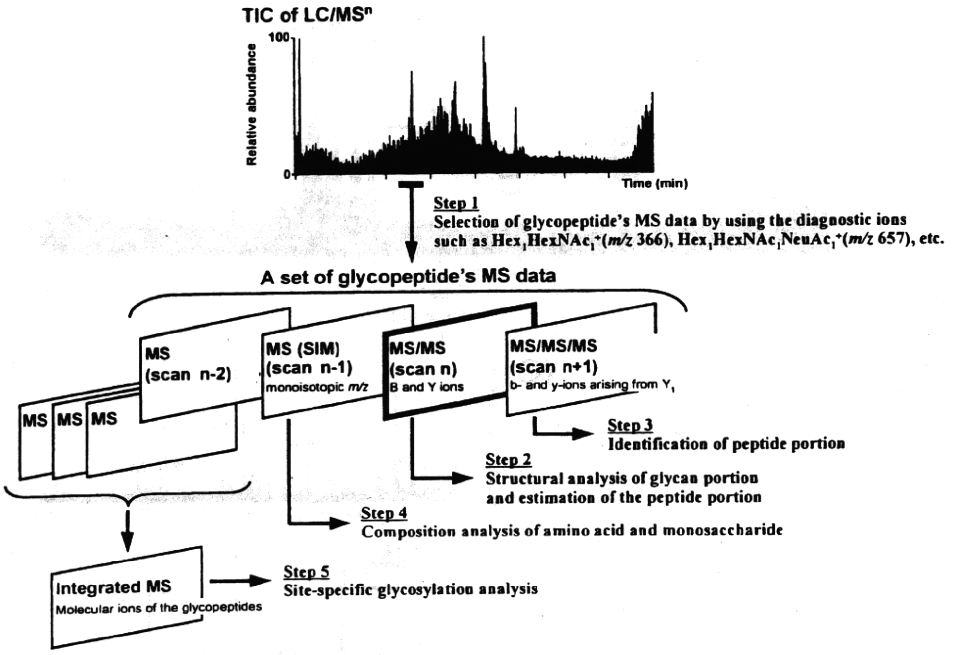


FIGURE 3: Methods used for LC−MS$^n$ and data analysis.

1) (step 3). The accurate molecular mass that was calculated from the monoisotopic *m/z* value and the charge state acquired by FT ICR-MS in SIM mode (scan $n$ − 1) was used to corroborate the assignment of the peptide and glycan moieties (step 4). The mass spectra acquired at the elution position, where the glycopeptides that yielded identical $Y_1$ ions in the MS/MS and/or MS/MS/MS spectra, were integrated, and the site-specific glycosylation was elucidated on the basis of the distribution of molecular ions in the integrated mass spectra (step 5). As a representative separation pattern, a total ion chromatogram (TIC) obtained by LC−MS$^n$ with a C30 column (scan range of *m/z* 1000−2000) is shown in Figure 4A. The MS/MS spectra containing the diagnostic ions at *m/z* 366 and 657 were picked out from all the MS data, and the peptides eluted at positions 1−25 were determined to be the glycopeptides on the basis of the carbohydrate-related ions. The 19% of spectra acquired at elution time, including positions 1−25, could be traced back to the glycopeptides of IgLON family proteins.

As for LAMP, it has seven potential N-glycosylation sites at Asn12, -38, -108, -120, -251, -259, and -272, and Asn287 is the predicted site of GPI linkage. On the basis of the presence of the peptide-related ions ([peptide + HexNAc + H]$^+$, $Y_1$ or $Y_{1\alpha/1\beta}$; or [peptide + dHex-HexNAc + H]$^+$, $Y_{1\alpha}$), glycopeptides that were eluted at the positions 1, 11, 14, 12, 4, and 24 were estimated to be the glycopeptides containing Asn12, -38, -108, -251, -259, and -272, respectively. The MS/MS spectra of the glycopeptide containing Asn120 (GSN$^{120}$VTLVCMANGRPE) were not acquired in any of the runs. However, glycosylation at Asn120 was confirmed by the detection of the peptide substituted with Asp (GSD$^{120}$VTLVCMANGRPEPVITWR) after PNGase F digestion (data not shown). Panels A1−F1 of Figure 5 show the representative MS/MS and MS/MS/MS spectra acquired at positions 11, 1, 14, 12, 4, and 24, respectively. The integrated mass spectra of the glycopeptides containing Asn38, -12, -108, -251, -259, and -272 are shown in panels A2−F2 of Figure 5, respectively. The feature of the glycosylation at each glycosylation site was elucidated on the basis of these MS spectra.

*(i) Asn38 (Asn43 in OBCAM and Asn38 in neurotrimin).* Panel A1 of Figure 5 shows one of the MS/MS spectra acquired at position 11. The peptide portion, VAWL(GlcNAc-)N$^{38}$R, was confirmed on the basis of the b- and y-ions that arose from $Y_1$ (*m/z* 961.5) in the MS/MS/MS spectrum (panel A1″ of Figure 5). A series of doubly charged Y ions with an *m/z* spacing pattern, 81 *m/z* units (Hex), suggests the linkage of Man-7 to this peptide. The attachment of Man-7 to VAWLN$^{38}$R, whose theoretical monoisotopic *m/z* value ([M + 2H]$^{2+}$) is 1149.983, was ascertained by the observed monoisotopic *m/z* value (1149.986) acquired in SIM mode on the FT ICR-MS (panel A1′ of Figure 5). Panel A2 of Figure 5 shows the integrated mass spectrum which was obtained from the mass spectra of glycopeptides that yielded $Y_1$ (*m/z* 961.5) via MS/MS. Four noticeable ion peaks (peaks a-1−a-4) appearing with the differences of 81 *m/z* units are assigned to VAWLN$^{38}$R glycosylated with Man-6-9 (Table 1A). The MS/MS spectra of DKNSKVAWLN$^{38}$R and CVVEDKNSKVAWLN$^{38}$R, which were picked out from positions 9 and 15, also revealed that Man-5, -7, and -8 were attached to Asn38.

*(ii) Asn12.* Panel B1 of Figure 5 shows the representative MS/MS spectrum of glycopeptide, GTDN$^{12}$ITVR, which was selected from position 1. From the $Y_{1\alpha}$ ion (*m/z* 1224.5) together with monoisotopic *m/z* value of the molecular ion (*m/z* 1173.132) and a series of doubly charged Y ions with an *m/z* spacing pattern, 146 (NeuAc), 101 (HexNAc), and 81 *m/z* units (Hex), the carbohydrate portion was estimated to be dHex$_1$Hex$_5$HexNAc$_4$NeuAc$_4$. Furthermore, a complex-type oligosaccharide, to which one branch of disialic acid was attached, was deduced from the presence of $B_{4\alpha}/Y_{5\alpha'}$ (*m/z* 495.3), $B_{2\alpha}$ (*m/z* 582.7), $B_{3\alpha}$ (*m/z* 744.9), $B_{4\alpha}/Y_{5\alpha''}$ and $B_{4\alpha}/Y_{7\alpha'}$ (*m/z* 948.2), and $B_{4\alpha}$ (*m/z* 1239.5) (inset of panel B1 of Figure 5). The integrated mass spectrum at position 1 suggests that the majority of the glycans at Asn12 are hybrid- and complex-type oligosaccharides containing disialic acids

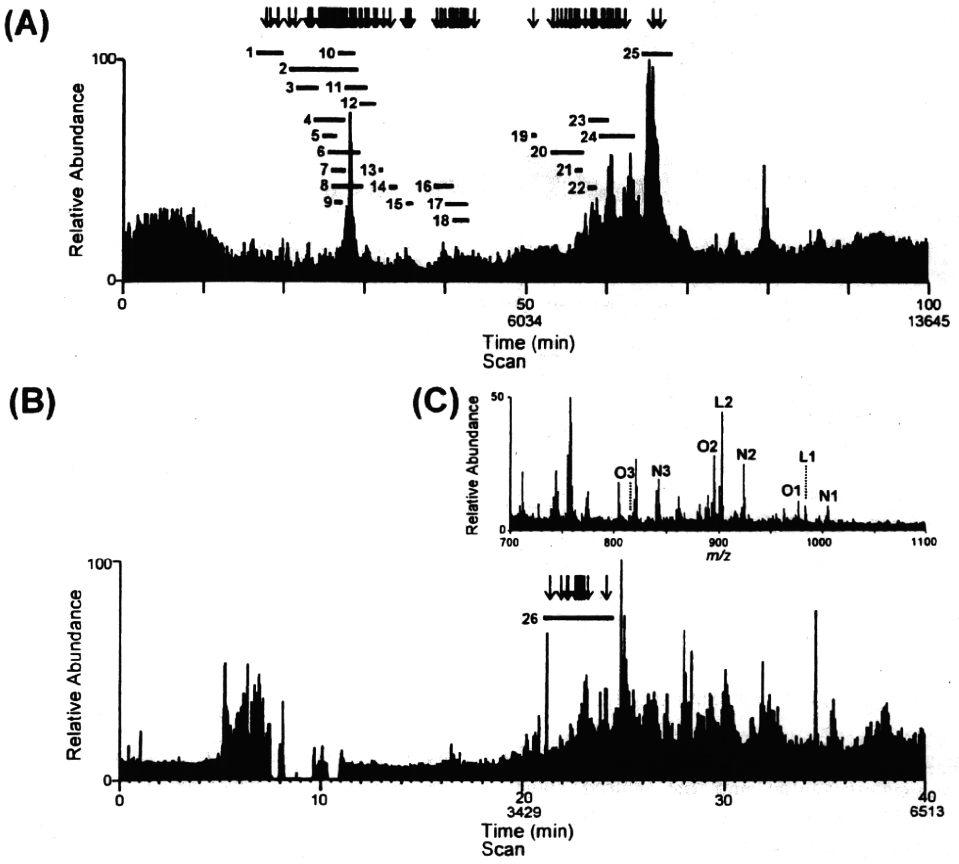


FIGURE 4: Total ion chromatograms obtained by C30-LC−MS$^n$ (A) and GCC-LC−MS$^n$ (B). Lines 1−25 and 26 are the elution positions of glycopeptides and GPI-linked peptides, respectively. The down arrow denotes the extracted position of the MS/MS spectra. (C) Integrated mass spectrum obtained from elution position 26. L1 and L2 are molecular ions of GPI-linked peptides from LAMP, N1−N3 those from neurotrimin, and O1−O3 those from OBCAM.

(panel B2 of Figure 5 and Table 1B). In addition, the partial glycosylation at Asn12 was indicated by the detection of nonglycosylated GTDN$^{12}$ITVR.

*(iii) Asn108.* The MS/MS spectrum of glycosylated ISN$^{108}$ISSDVTVNE ($Y_{1\alpha/1\beta}$, *m/z* 1480.6) acquired at position 14 is shown in panel C1 of Figure 5. The attachment of a Lewis a/x [Le$^{a/x}$, Gal-(Fuc-)GlcNAc-] or H antigen (Fuc-Gal-GlcNAc-) motif to the bisected complex-type oligosaccharide was deduced from the monosaccharide composition ($dHex_2Hex_4HexNAc_5$) and the Le$^{a/x}$ and H antigen-related ion (*m/z* 512.1) and $Y_{1\beta/3\alpha/3\beta}^{2+}$ (*m/z* 1024.3) (panel C1 of Figure 5, peak c-1 in panel C2 of Figure 5). The alternative LC−MS$^n$ run with the C30 column (scan range of *m/z* 1000−2000) suggested that ISN$^{108}$ISSD is also occupied by sialyl Le$^{a/x}$ (sLe$^{a/x}$)-modified or core-fucosylated hybrid-type oligosaccharides based on the presence of NeuAc-Hex-(dHex-)HexNAc$^+$ (*m/z* 803.1), Hex-(dHex-)HexNAc$^+$ (*m/z* 512.3), NeuAc-Hex$^+$ (*m/z* 454.2), and [peptide + dHex + HexNAc + H]$^+$ (*m/z* 1084.3) (data not shown, Table 1C).

*(iv) Asn251.* The representative MS/MS spectrum of the glycopeptide containing GQSSLTVTN$^{251}$VTE ($Y_{1\alpha/1\beta}$, *m/z* 1438.6; elution position 12) is shown in panel D1 of Figure 5. From the monoisotopic mass and the Le$^{a/x}$-related ions (*m/z* 350.3 and 512.2), the carbohydrate structure was estimated to be a complex-type oligosaccharide to which the Le$^{a/x}$ motif was attached ($dHex_2Hex_4HexNAc_5$; inset of panel D1 of Figure 5). Other glycans at Asn251 were characterized as complex-type oligosaccharides containing sLe$^{a/x}$ or Lewis b/y [Le$^{b/y}$, Fuc-Gal-(Fuc-)GlcNAc-] based on the molecular ions in the integrated mass spectrum (peaks d-1−6 in panel D2 of Figure 5), the sLe$^{a/x}$-related ions (*m/z* 803, 657, and 512), and the Le$^{b/y}$-related ions (*m/z* 658.2, 512.1, and 350.2) acquired by the alternative run with the C30 column (scan range of *m/z* 700−2000) (Table 1D).

*(v) Asn259.* Panel E1 of Figure 5 shows the product ion spectra of HYGN$^{259}$YTCVAANK linked by $dHex_1Hex_3HexNAc_5$, which was deduced from the $Y_{1\alpha/1\beta}$ ion (*m/z* 1600.6) and the monoisotopic mass acquired at position 4. The BA-2, which is a core-fucosylated and agalacto-biantennary oligosaccharide with bisecting GlcNAc, and known as a brain-specific carbohydrate, was suggested by the product ions at *m/z* 1085.3 (bisecting GlcNAc) and 1746.6 (core-fucosylation) (inset of panel E1 of Figure 5). The majority of other glycans at Asn259 were characterized as Le$^{a/x}$-modified complex and hybrid types. Man-5 was suggested to be a minor glycan (panel E2 of Figure 5 and Table 1E).

*(vi) Asn272.* Panel F1 of Figure 5 shows the MS/MS and MS/MS/MS spectra of glycopeptide LGVTN$^{272}$ASLVLFR ($Y_{1\alpha/1\beta}$, *m/z* 1492.8), which were acquired at position 24. The monosaccharide composition ($dHex_2Hex_4HexNAc_5$) and the presence of $Y_{3\alpha/3\beta}^{2+}$ (*m/z* 1103.8) and Le$^{a/x}$-related ion suggested the attachment of a Le$^{a/x}$ or H antigen motif to the bisected and core-fucosylated complex-type oligosaccharide (inset of panel F1 of Figure 5). The MS/MS spectra of the LGVTN$^{272}$ASLVLFRPGSVR glycopeptides ($Y_{1\alpha/1\beta}^{2+}$, *m/z* 1069) were also picked out at position 24 (data not shown). The *m/z* values of molecular ions appearing in the

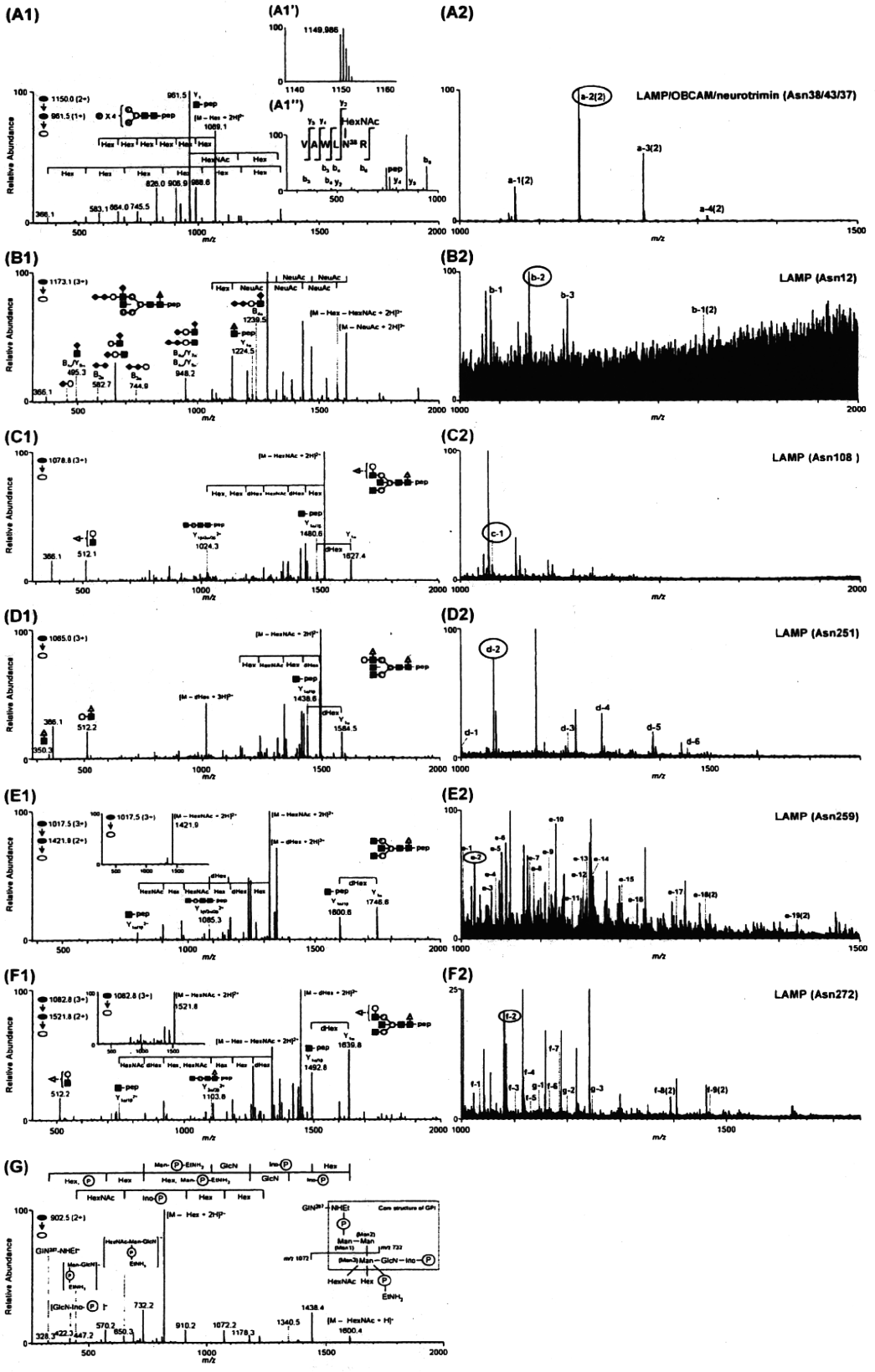


FIGURE 5: MS spectra of LAMP glycopeptides. (A1) MS/MS spectrum of glycopeptide VAWLN$^{38}$R; elution position, 11; precursor ion, $[M + 2H]^{2+}$ ($m/z$ 1150.0). (A1′) Mass spectrum on the FT ICR-MS in SIM mode. (A1″) MS/MS/MS spectrum acquired from $Y_1$ ($m/z$ 961.5). (A2) Integrated mass spectrum obtained from position 11. (B1) MS/MS spectrum of glycopeptide GTDN$^{12}$ITVR; elution position, 1; precursor ion, $[M + 3H]^{3+}$ ($m/z$ 1173.1). (B2) Integrated mass spectrum at position 1. (C1) MS/MS spectrum of glycopeptide ISN$^{108}$ISSDVTVNE; elution position, 14; precursor ion, $[M + 3H]^{3+}$ ($m/z$ 1078.8). (C2) Integrated mass spectrum at position 14. (D1) MS/MS spectrum of glycopeptide GQSSLTVTN$^{251}$VTE; elution position, 12; precursor ion, $[M + 3H]^{3+}$ ($m/z$ 1065.0). (D2) Integrated mass spectrum at position 12. (E1) MS/MS and MS/MS/MS spectra of glycopeptide HYGN$^{259}$YTCVAANK; elution position, 4; precursor ion, $[M + 3H]^{3+}$ ($m/z$ 1017.5). (E2) Integrated mass spectrum at position 4. (F1) MS/MS and MS/MS/MS spectra of glycopeptide LGVTN$^{272}$ASLVLFR; elution position, 24; precursor ion, $[M + 3H]^{3+}$ ($m/z$ 1082.8). (F2) Integrated mass spectrum at position 24. (G) MS/MS spectrum of GPI-linked GIN$^{287}$; elution position, 26; precursor ion, $[M + 2H]^{2+}$ ($m/z$ 902.5). Symbols are as in Figure 9.

Table 1: Summary of Glycosylation Analysis of IgLON Family Proteins

| | peptides | | glycopeptides | | | | | | *N*-glycan | | | | |
|---|---|---|---|---|---|---|---|---|---|---|---|---|---|
| | | | | | | | | | deduced monosaccharide composition | | | | |
| protein | | sequence[a,b] | elution position | Figure | peak no.[c] | scan in Figure 4A[d] | observed peptide-related ion[e] | observed *m/z* in SIM mode[b] | theoretical *m/z*[b] | dHex | Hex | HexNAc | NA | deduced structure[f] (diagnostic ion) |
| LAMP | B | GTDN[12]ITVR (874.451) | 1 | 5, B2 | b-1 | 2095 (A, B) | 1225.4 | 1076.101 (3) | 1076.101 | 1 | 5 | 4 | 2 | H, CoreF(1225.4) |
| | | | | | b-1 (2) | 2146 | 1225.6 | 1613.652 (2) | 1613.648 | 1 | 5 | 4 | 2 | H, CoreF(1225.6) |
| | | | | | **b-2** | **2166 (A, B, C)** | **1224.5** | **1173.132 (3)** | **1173.133** | **1** | **5** | **4** | **3** | **H, CoreF(1224.5), diSia(582.7) [Figure 5, B1]** |
| | | | | | | – (A) | 1224.5 | 1759.195 (2) | 1759.196 | 1 | 5 | 4 | 3 | CoreF(1224.5), diSia(583.0) |
| | | | | | b-3 | 2235 (A) | 1224.5 | 1270.166 (3) | 1270.165 | 1 | 5 | 4 | 4 | C, CoreF(1224.5), diSia(583.0) |
| | | | | | | – (A) | 1225.6 | 1367.199 (3) | 1367.196 | 1 | 5 | 4 | 5 | C, CoreF(1225.6), diSia(583.4) |
| | A | VAWLN[38]R (757.424) | 11 | 5, A2 | | – (B) | 961.5 | 987.930 (2) | 987.930 | 0 | 5 | 2 | 0 | Man-5 |
| | | | | | a-1 (2) | 3523 (A, B, C) | 961.5 | 1068.956 (2) | 1068.957 | 0 | 6 | 2 | 0 | Man-6 |
| | | | | | **a-2 (2)** | **3364 (A, B, C)** | **961.5** | **1149.986(2)** | **1149.983** | **0** | **7** | **2** | **0** | **Man-7 [Figure 5, A1]** |
| | | | | | a-3 (2) | 3221 (A, B, C) | 961.5 | 1231.010 (2) | 1231.010 | 0 | 8 | 2 | 0 | Man-8 |
| | | | | | a-4 (2) | 3413 (A, B, C) | 961.5 | 1312.039 (2) | 1312.036 | 0 | 9 | 2 | 0 | Man-9 |
| | | DKNSKVAWLN[38]R (1329.715) | 9 | – | – | 3074 | 1534.8 | 1011.774 (3) | 1011.773 | 0 | 8 | 2 | 0 | Man-8 |
| | | CVVEDKNSKVAWLN[38]R (1816.925) | 15 | – | – | 4298 | 675.5(3) | 1012.128 (3) | 1012.123 | 0 | 5 | 2 | 0 | Man-5 |
| | | | | | – | 4245 | 1011.2(2) | 1120.160 (3) | 1120.159 | 0 | 7 | 2 | 0 | Man-7 |
| | | | | | – | 4208 | 1011.3(2) | 1174.175 (3) | 1174.176 | 0 | 8 | 2 | 0 | Man-8 |
| | C | ISN[108]ISSD (734.345) | – | – | | – (A) | 938.4 | 1296.508 (2) | 1296.507 | 1 | 5 | 3 | 1 | H, CoreF(1084.3) or $sL^{a/x}$ (454.2, 512.3, 657.2, 803.1) |
| | | | | | | – (A) | 938.5 | 1377.533 (2) | 1377.534 | 1 | 6 | 3 | 1 | H, CoreF(1084.2) |
| | | ISN[108]ISSDVTVNE (1276.615) | 14 | 5, C2 | **c-1** | **3963** | **1480.6** | **1078.456 (3)** | **1078.454** | **2** | **4** | **5** | **0** | **C, CoreF(1627.4), bisectGN(1024.3) [Figure 5, C1]** |
| | | GSN[120]VTLVCMANGRPEPVITWR (1603.745) | – | – | – | – | – | – | – | – | – | – | – | glycosylated [g] |
| | D | GQSSLTVTN[251]VTE (1234.604) | 12 | 5, D2 | | – (A) | 1438.6 | 1340.576 (2) | 1340.576 | 1 | 3 | 4 | 0 | CoreF(1584.6), bisectGN(1003.6) |
| | | | | | | – (A) | 1438.5 | 961.746 (3) | 961.746 | 1 | 3 | 5 | 0 | C, CoreF(1584.5), bisectGN(1004.1), BA-2 |
| | | | | | | – (A, B) | 1438.5 | 1442.115 (2) | 1442.116 | 1 | 3 | 5 | 0 | C, CoreF(1584.5), bisectGN(1077.2), BA-2 |
| | | | | | d-1 | 3630 | 1438.5 | 1002.088 (3) | 1002.088 | 1 | 5 | 4 | 0 | H, CoreF(1584.5) or $L^{a/x}$ (350.1, 512.1) |
| | | | | | **d-2** | **3646 (A, B, C)** | **1438.6** | **1064.451 (3)** | **1064.450** | **2** | **4** | **5** | **0** | **C, CoreF(1584.5), $L^{a/x}$ (350.3, 512.2) [Figure 5, D1]** |
| | | | | | | – (C) | 1439.6 | 1596.174 (2) | 1596.171 | 2 | 4 | 5 | 0 | C, CoreF(1585.6), 512(512.2) |
| | | | | | | – (B) | 1438.5 | 1167.154 (3) | 1167.154 | 3 | 5 | 5 | 0 | C, CoreF(1584.5), bisectGN(1004.1), $L^{b/y}$ (350.2, 512.1, 658.2) |
| | | | | | d-3 | 3742 (C) | 1438.6 | 1215.502 (3) | 1215.499 | 2 | 5 | 5 | 1 | C, CoreF(1584.4), 512(512.3) |
| | | | | | d-4 | 3788 (C) | 1438.6 | 1283.192 (3) | 1283.193 | 2 | 5 | 6 | 1 | C, CoreF(1584.5) ($sL^{a/x}$ (512.2, 657.2, 803.2)) |
| | | | | | d-5 | 3668 | 1438.6 | 1385.898 (3) | 1385.896 | 3 | 6 | 6 | 1 | C, CoreF(1584.5) ($sL^{a/x}$ (512.2, 657.3, 803.1)) |
| | | | | | d-6 | 3618 (A) | 1438.5 | 1453.594 (3) | 1453.589 | 3 | 6 | 7 | 1 | C, CoreF(1584.6), 512(512.2) |

Table 1: Continued

| protein | peptides: sequence[a,b] | elution position | Figure | peak no.[c] | scan in Figure 4A[d] | observed peptide-related ion[e] | observed *m/z* in SIM mode[b] | theoretical *m/z*[b] | *N*-glycan: deduced monosaccharide composition: dHex | Hex | HexNAc | NA | deduced structure[f] (diagnostic ion) |
|---|---|---|---|---|---|---|---|---|---|---|---|---|---|
| E | HYGN[259]YTCVAANK (1396.619) | 4 | 5, E2 | | – (B) | 801.8(2) | 872.021 (3) | 872.021 | 0 | 5 | 2 | 0 | Man-5 |
| | | | | e-18 (2) | 2884 | 1600.6 | 1307.532 (2) | 1307.528 | 0 | 5 | 2 | 0 | Man-5 |
| | | | | e-19 (2) | 2949 (A) | 1601.4 | 1421.587 (2) | 1421.584 | 1 | 3 | 4 | 0 | CoreF(1746.7), bisectGN(1085.6) |
| | | | | e-1 | 2891 (A, C) | 1600.6 | 1002.079 (3) | 1002.076 | 1 | 4 | 4 | 0 | H, CoreF(1746.6), bisectGN(1085.3) |
| | | | | **e-2** | **2931 (A, B, C)** | **1600.6** | **1015.752 (3)** | **1015.752** | **1** | **3** | **5** | **0** | **C, CoreF(1746.6), bisectGN(1085.3), BA-2 [Figure 5, E1]** |
| | | | | e-3 | 2859 (A) | 1600.5 | 1037.089 (3) | 1037.086 | 2 | 5 | 3 | 0 | H, CoreF(1746.6), 512(512.1) |
| | | | | e-4 | 2840 | 1600.6 | 1042.419 (3) | 1042.418 | 1 | 6 | 3 | 0 | H, 512(512.1) |
| | | | | e-5 | 2878 (A) | 1601.6 | 1050.764 (3) | 1050.762 | 2 | 4 | 4 | 0 | CoreF(1746.6), $L^{a/x}$ (350.2, 512.2), bisectGN(1085.5) |
| | | | | e-6 | 2853 (A, B, C) | 1600.5 | 1056.095 (3) | 1056.094 | 1 | 5 | 4 | 0 | H, CoreF(1747.7), bisectGN(1085.6) |
| | | | | e-7 | 2994 | 1600.7 | 1085.433 (3) | 1085.432 | 1 | 5 | 3 | 1 | H, CoreF(1747.6) or 512(512.2) |
| | | | | e-8 | 2821 | 1600.5 | 1091.107 (3) | 1091.104 | 2 | 6 | 3 | 0 | H, CoreF(1746.6), 512(512.2) |
| | | | | | – (A, C) | 1601.6 | 1104.779 (3) | 1104.780 | 2 | 5 | 4 | 0 | H, CoreF(1747.8), bisectGN(1158.7), $L^{a/x}$ (349.9, 512.3) |
| | | | | e-9 | 2847 | 1600.6 | 1110.111 (3) | 1110.111 | 1 | 6 | 4 | 0 | H, CoreF(1746.6) or $L^{a/x}$ (350.1, 512.3) |
| | | | | e-10 | 2898 (A, C) | 1601.7 | 1118.457 (3) | 1118.455 | 2 | 4 | 5 | 0 | C, CoreF(1746.7), bisectGN(1085.7), $L^{a/x}$ (350.2, 512.1) |
| | | | | e-11 | 2989 | 1600.7 | 1139.452 (3) | 1139.450 | 1 | 6 | 3 | 1 | H, CoreF(1746.7) |
| | | | | e-12 | 2808 (A) | 1600.6 | 1153.467 (3) | 1153.466 | 3 | 5 | 4 | 0 | C, CoreF(1746.6), $L^{b/y}$ (658.2) or 512/512(512.1/512.3) |
| | | | | e-13 | 2872 | 1600.4 | 1158.798 (3) | 1158.797 | 2 | 6 | 4 | 0 | H, CoreF(1747.7), $L^{a/x}$ (350.1, 512.1) |
| | | | | e-14 | 3036 | 1601.7 | 1166.800 (3) | 1166.801 | 1 | 4 | 5 | 1 | C, CoreF(1747.4) or 512(512.1), bisectGN(1085.3) |
| | | | | e-15 | 2983 | 1600.6 | 1201.813 (3) | 1201.811 | 2 | 5 | 4 | 1 | C, CoreF(1747.6), $sL^{a/x}$ (350.1, 512.2, 657.3, 803.2) |
| | | | | e-16 | 2815 | 1600.6 | 1221.160 (3) | 1221.159 | 3 | 5 | 5 | 0 | C, CoreF(1747.6), bisectGN(1085.3), 512(512.2) |
| | | | | e-17 | 3013 | 1600.7 | 1269.507 (3) | 1269.505 | 2 | 5 | 5 | 1 | C, CoreF(1746.7), bisectGN(1085.5), 512(512.1) |

Table 1: Continued

| protein | peptides: sequence[a,b] | elution position | Figure | peak no.[c] | scan in Figure 4A[d] | observed peptide-related ion[e] | observed *m/z* in SIM mode[b] | theoretical *m/z*[b] | *N*-glycan: deduced monosaccharide composition dHex | Hex | HexNAc | NA | deduced structure[f] (diagnostic ion) |
|---|---|---|---|---|---|---|---|---|---|---|---|---|---|
| F | LGVTN[272]ASLVLFR (1288.750) | 24 | 5, F2 | | – (B) | 1492.8 | 931.109 (3) | 1396.160 | 0 | 3 | 5 | 0 | C, bisectGN(1030.9) |
| | | | | f-8 (2) | 7644 (A, B) | 1492.8 | 1396.161 (2) | 1396.160 | 0 | 3 | 5 | 0 | C, bisectGN(1031.0) |
| | | | | | – (B) | 1492.8 | 979.795 (3) | 979.795 | 1 | 3 | 5 | 0 | C, CoreF(1638.9), bisectGN(1031.2), BA-2 |
| | | | | f-9 (2) | 7577 (A, B, C) | 1492.7 | 1469.189 (2) | 1469.189 | 1 | 3 | 5 | 0 | C, CoreF(1638.8), bisectGN(1031.2), BA-2 |
| | | | | | – (A, B, C) | 1492.9 | 1014.806 (3) | 1014.806 | 2 | 4 | 4 | 0 | C, CoreF(1640.0), 512(512.3) |
| | | | | f-1 | 7558 (A, B, C) | 1493.7 | 1033.813 (3) | 1033.813 | 1 | 4 | 5 | 0 | C, bisctGN(1031.1), CoreF(1639.8) or $L^{a/x}$ (350.2, 512.2) |
| | | | | | – (A) | 1493.8 | 1550.215 (2) | 1550.215 | 1 | 4 | 5 | 0 | C, bisctGN(1031.6), CoreF(1640.0) or 512(512.2) |
| | | | | | – (A) | 1492.9 | 1047.489 (3) | 1047.488 | 1 | 3 | 6 | 0 | C, CoreF(1638.8), bisectGN(1031.7) |
| | | | | | – (A, C) | 1492.9 | 1063.151 (3) | 1063.151 | 1 | 4 | 4 | 1 | C, CoreF(1638.9) |
| | | | | | – (A) | 1492.9 | 1082.157 (3) | 1082.159 | 0 | 4 | 5 | 1 | C, bisectGN(1031.0) |
| | | | | **f-2** | **7468 (A, B, C)** | **1492.8** | **1082.499 (3)** | **1082.499** | **2** | **4** | **5** | **0** | **C, CoreF, bisectGN(1103.8) [Figure 5, F1]** |
| | | | | | – (A) | 1492.8 | 1623.243 (2) | 1623.244 | 2 | 4 | 5 | 0 | C, CoreF(1638.9), bisectGN(1031.0), 512(513.2) |
| | | | | f-3 | 7382 (A) | 1492.8 | 1101.510 (3) | 1101.506 | 1 | 4 | 6 | 0 | C, bisectGN(1031.2), CoreF(1639.0) or $L^{a/x}$ (350.3, 512.2) |
| | | | | f-4 | 7753 (A, B, C) | 1492.7 | 1117.168 (3) | 1117.169 | 1 | 5 | 4 | 1 | C, CoreF(1638.8) or $sL^{a/x}$ (454.2, 512.3, 657.2, 803.1) |
| | | | | | – (A) | 1493.9 | 1675.247 (2) | 1675.250 | 1 | 5 | 4 | 1 | H, CoreF(1638.9) |
| | | | | | – (A) | 1493.8 | 1117.508 (3) | 1117.509 | 3 | 5 | 4 | 0 | C, CoreF(1639.4), $L^{b/y}$ (512.2, 658.5) |
| | | | | f-5 | 7889 (A, C) | 1492.8 | 1130.846 (3) | 1130.845 | 1 | 4 | 5 | 1 | C, CoreF(1638.7), bisectGN(1031.0, 1104.3) |
| | | | | | – (A) | 1492.9 | 1136.517 (3) | 1136.516 | 2 | 5 | 5 | 0 | C, CoreF(1639.8), 512(512.2) |
| | | | | | – (A) | 1494.0 | 1150.192 (3) | 1150.192 | 2 | 4 | 6 | 0 | C, CoreF(1639.1), $L^{a/x}$ (350.1, 512.2) |
| | | | | | – (A) | 1493.1 | 1165.516 (3) | 1165.515 | 0 | 5 | 4 | 2 | C |
| | | | | f-6 | 7815 (A, B, C) | 1492.6 | 1165.856 (3) | 1165.855 | 2 | 5 | 4 | 1 | C, CoreF(1638.7), $sL^{a/x}$ (453.8, 512.1, 657.1, 803.2) |
| | | | | | – (A) | 1493.3 | 1748.280 (2) | 1748.279 | 2 | 5 | 4 | 1 | C, CoreF(1639.9), 512(512.3) |
| | | | | f-7 | 7765 | 1493.9 | 1184.864 (3) | 1184.862 | 1 | 5 | 5 | 1 | C, bisectGN(1032.0), CoreF(1639.3) or 512(512.2) |
| | | | | | – (A, C) | 1492.7 | 1185.202 (3) | 1185.202 | 3 | 5 | 5 | 0 | C, CoreF(1639.1), $L^{b/y}$ (512.2, 658.4) |
| | | | | | – (A) | 1492.7 | 1204.209 (3) | 1204.209 | 2 | 5 | 6 | 0 | C, CoreF(1638.9), $L^{a/x}$ (350.2, 512.2) |
| | | | | | – (A, C) | 1493.2 | 1214.201 (3) | 1214.201 | 1 | 5 | 4 | 2 | C, CoreF(1639.8) |

Table 1: Continued

| protein | peptides | | glycopeptides | | | | | | | *N*-glycan | | | | |
|---|---|---|---|---|---|---|---|---|---|---|---|---|---|---|
| | | | | | | | | | | deduced monosaccharide composition | | | | |
| | | sequence[a,b] | elution position | Figure | peak no.[c] | scan in Figure 4A[d] | observed peptide-related ion[e] | observed *m/z* in SIM mode[b] | theoretical *m/z*[b] | dHex | Hex | HexNAc | NA | deduced structure[f] (diagnostic ion) |
| | | | | | | – (A) | 1493.8 | 1233.548 (3) | 1233.548 | 2 | 5 | 5 | 1 | C, CoreF(1639.1), sL$^{a/x}$ (454.0, 512.6, 657.1, 803.0) |
| | | | | | | – (A) | 1493.8 | 1287.567 (3) | 1287.566 | 2 | 6 | 5 | 1 | C, CoreF(1639.4), 512(512.3) |
| | | | | | | – (C) | 1492.7 | 1336.251 (3) | 1336.252 | 3 | 6 | 5 | 1 | C, CoreF, 512(512.4) |
| | | | | | | - (C) | 1492.7 | 1384.602 (3) | 1384.598 | 2 | 6 | 5 | 2 | C, CoreF(1638.8) (sL$^{a/x}$ (454.9, 512.3, 657.1, 803.3)) |
| | | LGVTN$^{272}$ASLVLFRPGSVR (1785.026) | 24 | 5, F2 | | – (C) | 995.3(2) | 1096.537 (3) | 1096.534 | 0 | 3 | 5 | 0 | C, bisectGN(1279.5) |
| | | | | | g-1 | 7508 (C) | 995.4(2) | 1145.223 (3) | 1145.220 | 1 | 3 | 5 | 0 | C, CoreF(1068.7), bisectGN(1352.3), BA-2 |
| | | | | | g-2 | 7462 (C) | 995.8(2) | 1199.243 (3) | 1199.238 | 1 | 4 | 5 | 0 | C, CoreF(1069.2) or 512(512.2) |
| | | | | | g-3 | 7449 (C) | 995.9(2) | 1247.927 (3) | 1247.924 | 2 | 4 | 5 | 0 | C, CoreF(1068.4), bisectGN(1279.4), 512(512.2) |
| | | | | | | – (C) | 995.8(2) | 1282.596 (3) | 1282.594 | 1 | 5 | 4 | 1 | C, 512(512.2) |
| | | | | | | – (C) | 995.4(2) | 1331.283 (3) | 1331.280 | 2 | 5 | 4 | 1 | C, CoreF(1068.4), 512(512.3) |
| OBCAM | G | AMDN$^{17}$VTVR (904.444) | 2 | 6, A2 | h-1 | 2408 (A) | 1254.5 | 1018.407 (3) | 1018.405 | 1 | 5 | 3 | 2 | H, CoreF(1254.5), (diSia(583.0)) |
| | | | | | | – (A, C) | 1254.7 | 1086.098 (3) | 1086.099 | 1 | 5 | 4 | 2 | CoreF(1254.7) |
| | | | | | | – (A) | 1254.5 | 1628.644 (2) | 1628.644 | 1 | 5 | 4 | 2 | C, CoreF(1254.5) |
| | | | | | | – (A, B) | 1254.7 | 1115.437 (3) | 1115.437 | 1 | 5 | 3 | 3 | H, CoreF(1254.7), diSia(583.0) |
| | | | | | | – (A) | 1254.5 | 1672.651 (2) | 1672.652 | 1 | 5 | 3 | 3 | H, CoreF(1254.5), diSia(583.3) |
| | | | | | | – (A) | 1254.6 | 1169.454 (3) | 1169.455 | 1 | 6 | 3 | 3 | H, CoreF(1254.6), diSia(583.0) |
| | | | | | h-2 | 2473 (A, B, C) | 1254.5 | 1183.131 (3) | 1183.130 | 1 | 5 | 4 | 3 | H, CoreF(1254.5) or 512(512.2), diSia(582.6) |
| | | | | | **h-3** | **2719 (C)** | **1254.5** | **1280.163 (3)** | **1280.162** | **1** | **5** | **4** | **4** | **C, CoreF(1254.5), diSia(582.9) [Figure 6, A1]** |
| | | | | | | – (C) | 1108.6 | 1377.198 (3) | 1377.194 | 1 | 5 | 4 | 5 | |
| | A | VAWLN$^{43}$R (757.424) | 11 | 5, A2 | | – (B) | 961.5 | 987.930 (2) | 987.930 | 0 | 5 | 2 | 0 | Man-5 |
| | | | | | a-1 (2) | 3523 (A, B, C) | 961.5 | 1068.956 (2) | 1068.957 | 0 | 6 | 2 | 0 | Man-6 |
| | | | | | **a-2 (2)** | **3364 (A, B, C)** | **961.5** | **1149.986(2)** | **1149.983** | **0** | **7** | **2** | **0** | **Man-7 [Figure 5, A1]** |
| | | | | | a-3 (2) | 3221 (A, B, C) | 961.5 | 1231.010 (2) | 1231.010 | 0 | 8 | 2 | 0 | Man-8 |
| | | | | | a-4 (2) | 3413 (A, B, C) | 961.5 | 1312.039 (2) | 1312.036 | 0 | 9 | 2 | 0 | Man-9 |
| | | VHLIVQVPPQIMN$^{113}$ISSD (1889.008) | – | – | – | – | – | – | – | – | – | – | – | glycosylated [g] |
| | | VHLIVQVPPQIMN$^{113}$ISSDITVNE (2445.294) | – | – | – | – | – | – | – | – | – | – | – | glycosylated [g] |
| | H | ISTLTFFN$^{258}$VSE (1256.629) | 25 | 6, B2 | | – (A) | 1460.6 | 1351.589 (2) | 1351.589 | 1 | 3 | 4 | 0 | CoreF(1606.3), bisectGN(1087.8) |
| | | | | | | – (B) | 1460.5 | 969.088 (3) | 969.088 | 1 | 3 | 5 | 0 | C, CoreF(1606.5), bisectGN(1088.6), BA-2 |
| | | | | | | – (A, C) | 1461.5 | 1453.128 (2) | 1453.128 | 1 | 3 | 5 | 0 | C, CoreF(1606.5), bisectGN(1088.4), BA-2 |

Table 1: Continued

| protein | peptides: sequence[a,b] | elution position | Figure | glycopeptides: peak no.[c] | scan in Figure 4A[d] | observed peptide-related ion[e] | observed m/z in SIM mode[b] | theoretical m/z[b] | N-glycan: deduced monosaccharide composition dHex | Hex | HexNAc | NA | deduced structure[f] (diagnostic ion) |
|---|---|---|---|---|---|---|---|---|---|---|---|---|---|
| | | | | | − (A, B, C) | 1461.7 | 1071.792 (3) | 1071.792 | 2 | 4 | 5 | 0 | C, (CoreF(1606.5), $L^{a/x}$ (350.1, 512.2)) or ($L^{b/y}$ (658.4)) |
| | | | | | − (A, C) | 1460.5 | 1607.183 (2) | 1607.184 | 2 | 4 | 5 | 0 | C, 512(512.3) |
| | | | | | − (C) | 1460.5 | 1120.138 (3) | 1120.137 | 1 | 4 | 5 | 1 | C, CoreF(1606.5) |
| | | | | | − (A, C) | 1460.5 | 1155.148 (3) | 1155.148 | 2 | 5 | 4 | 1 | C, CoreF(1606.6) ($sL^{a/x}$ (349.2, 512.2, 804.1) |
| | | | | | − (A, B) | 1460.5 | 1174.494 (3) | 1174.495 | 3 | 5 | 5 | 0 | C, CoreF(1606.5), $L^{b/y}$ (350.7, 512.3, 658.2) |
| | | | | | − (A, C) | 1461.4 | 1187.831 (3) | 1187.831 | 1 | 4 | 6 | 1 | C, CoreF(1606.6) or $sL^{a/x}$ (350.1, 512.5, 657.1, 803.1) |
| | | | | | − (C) | 1460.5 | 1222.842 (3) | 1222.841 | 2 | 5 | 5 | 1 | C, CoreF(1606.5), $sL^{a/x}$ (454.0, 512.2, 803.2) |
| | | | | **i-1** | **8712 (A, B, C)** | **1460.5** | **1290.538 (3)** | **1290.534** | **2** | **5** | **6** | **1** | **C, CoreF(1606.6) ($sL^{a/x}$ (454.2, 512.2, 657.1, 803.3) [Figure 6, B1]** |
| | | | | i-2 | 8541 (A, C) | 1460.5 | 1393.239 (3) | 1393.238 | 3 | 6 | 6 | 1 | C, CoreF(1606.5), 512(512.2) |
| 1 | YGN[266]YTCVATNK (1289.571) | 7 | 6, C2 | | − (A) | 1493.6 | 1254.003 (2) | 1254.004 | 0 | 5 | 2 | 0 | Man-5 |
| | | | | | − (A) | 1493.6 | 1368.060 (2) | 1368.060 | 1 | 3 | 4 | 0 | CoreF(1639.6), bisectGN(1031.5) |
| | | | | | − (B) | 1493.6 | 980.068 (3) | 980.069 | 1 | 3 | 5 | 0 | C, CoreF(1639.6), bisectGN(1032.2), BA-2 |
| | | | | j-4 (2) | 3156 (A, B, C) | 1493.6 | 1469.602 (2) | 1469.599 | 1 | 3 | 5 | 0 | C, CoreF(1639.6), bisectGN(1105.0), BA-2 |
| | | | | | − (C) | 1493.6 | 1015.082 (3) | 1015.079 | 2 | 4 | 4 | 0 | CoreF(1639.5), $L^{a/x}$ (350.2, 512.1), bisectGN(1105.1) |
| | | | | j-1 | 3048 (A) | 1494.6 | 1082.774 (3) | 1082.772 | 2 | 4 | 5 | 0 | C, CoreF(1640.5), $L^{a/x}$ (350.4, 512.2), bisectGN(1105.9) **[Figure 6, C1]** |
| | | | | j-2 | 3030 | 1493.6 | 1117.783 (3) | 1117.783 | 3 | 5 | 4 | 0 | H, CoreF(1639.5), $L^{b/y}$ (350.3, 512.1, 658.1) |
| | | | | j-3 | 3024 | 1494.6 | 1185.478 (3) | 1185.476 | 3 | 5 | 5 | 0 | C, CoreF(1639.6), $L^{a/x}$ (349.0, 512.1), bisectGN(1032.7) |
| | DYGN[266]YTCVATNK (1404.598) | 13 | − | | − (A) | 1608.6 | 1311.517 (2) | 1311.518 | 0 | 5 | 2 | 0 | Man-5 |
| | | | | | 3885 (A) | 1609.7 | 1018.412 (3) | 1018.411 | 1 | 3 | 5 | 0 | C, CoreF(1754.5), bisectGN(1089.6), BA-2 |
| | | | | | − (A) | 1608.6 | 1527.113 (2) | 1527.113 | 1 | 3 | 5 | 0 | C, CoreF(1754.6), bisectGN(1089.1), BA-2 |
| | | | | | − (A) | 1608.6 | 1121.115 (3) | 1121.115 | 2 | 4 | 5 | 0 | C, CoreF(1754.7), $L^{a/x}$ (350.3, 512.3) |
| | | | | | − (A) | 1608.7 | 1156.125 (3) | 1156.125 | 3 | 5 | 4 | 0 | H, CoreF(1754.8), 512(512.2) |
| | KDYGN[266]YTCVATNK (1532.693) | 6 | − | | − (C) | 1736.7 | 1489.625 (2) | 1489.621 | 1 | 3 | 4 | 0 | CoreF(1882.8), bisectGN(1225.1) |
| | | | | | 3510 (C) | 1737.8 | 1061.109 (3) | 1061.109 | 1 | 3 | 5 | 0 | C, CoreF(1884.9), bisectGN(1226.7), BA-2 |
| | | | | | 3133 | 1737.7 | 1150.141 (3) | 1150.137 | 2 | 5 | 4 | 0 | H, CoreF(1883.8), $L^{a/x}$ (350.4, 512.2) |

Table 1: Continued

| protein | peptides | | | glycopeptides | | | | | | *N*-glycan | | | | |
|---|---|---|---|---|---|---|---|---|---|---|---|---|---|---|
| | | | | | | | | | | deduced monosaccharide composition | | | | |
| | | sequence[a,b] | elution position | Figure | peak no.[c] | scan in Figure 4A[d] | observed peptide-related ion[e] | observed *m/z* in SIM mode[b] | theoretical *m/z*[b] | dHex | Hex | HexNAc | NA | deduced structure[f] (diagnostic ion) |
| | | | | | | − (C) | 1736.5 | 1163.814 (3) | 1163.813 | 2 | 4 | 5 | 0 | C, CoreF(1882.7), bisectGN(1153.7), $L^{a/x}$ (350.3, 512.2) |
| | | | | | | 3054 | 1737.6 | 1198.826 (3) | 1198.823 | 3 | 5 | 4 | 0 | C, CoreF(1884.7), $L^{a/x}$ (350.1, 512.2) |
| | | | | | | 3458 | 1737.1 | 1212.160 (3) | 1212.159 | 1 | 4 | 5 | 1 | C, CoreF(1883.9), bisectGN(1226.3) |
| | | | | | | 3295 | 1737.0 | 1247.170 (3) | 1247.169 | 2 | 5 | 4 | 1 | CoreF(1882.8), $sL^{a/x}$ (453.8, 512.2, 657.2, 803.2) |
| | J | LGNTN[279]ASITLYGPGAVID (1774.910) | – | – | | − (A) | 1978.7 | 1093.161 (3) | 1093.162 | 0 | 3 | 5 | 0 | C |
| | | | | | | − (A) | 1979.8 | 1141.848 (3) | 1141.848 | 1 | 3 | 5 | 0 | C, CoreF(1062.9), bisectGN(1273.8), BA-2 |
| neurotrimin | G | AMDN[12]VTVR (904.444) | 2 | 6, A2 | h-1 | 2408 (A) | 1254.5 | 1018.407 (3) | 1018.405 | 1 | 5 | 3 | 2 | H, CoreF(1254.5), (diSia(583.0)) |
| | | | | | | − (A, C) | 1254.7 | 1086.098 (3) | 1086.099 | 1 | 5 | 4 | 2 | CoreF(1254.7) |
| | | | | | | − (A) | 1254.5 | 1628.644 (2) | 1628.644 | 1 | 5 | 4 | 2 | C, CoreF(1254.5) |
| | | | | | | − (A, B) | 1254.7 | 1115.437 (3) | 1115.437 | 1 | 5 | 3 | 3 | H, CoreF(1254.7), diSia(583.0) |
| | | | | | | − (A) | 1254.5 | 1672.651 (2) | 1672.652 | 1 | 5 | 3 | 3 | H, CoreF(1254.5), diSia(583.3) |
| | | | | | | − (A) | 1254.6 | 1169.454 (3) | 1169.455 | 1 | 6 | 3 | 3 | H, CoreF(1254.6), diSia(583.0) |
| | | | | | h-2 | 2473 (A, B, C) | 1254.5 | 1183.131 (3) | 1183.130 | 1 | 5 | 4 | 3 | H, CoreF(1254.5) or 512(512.2), diSia(582.6) |
| | | | | | **h-3** | **2719 (C)** | **1254.5** | **1280.163 (3)** | **1280.162** | **1** | **5** | **4** | **4** | **C, CoreF(1254.5), diSia(582.9) [Figure 6, A1]** |
| | | | | | | − (C) | 1108.6 | 1377.198 (3) | 1377.194 | 1 | 5 | 4 | 5 | |
| | A | VAWLN[38]R (757.424) | 11 | 5, A2 | * | − (B) | 961.5 | 987.930 (2) | 987.930 | 0 | 5 | 2 | 0 | Man-5 |
| | | | | | a-1 (2) | 3523 (A, B, C) | 961.5 | 1068.956 (2) | 1068.957 | 0 | 6 | 2 | 0 | Man-6 |
| | | | | | **a-2 (2)** | **3364 (A, B, C)** | **961.5** | **1149.986(2)** | **1149.983** | **0** | **7** | **2** | **0** | **Man-7 [Figure 5, A1]** |
| | | | | | a-3 (2) | 3221 (A, B, C) | 961.5 | 1231.010 (2) | 1231.010 | 0 | 8 | 2 | 0 | Man-8 |
| | | | | | a-4 (2) | 3413 (A, B, C) | 961.5 | 1312.039 (2) | 1312.036 | 0 | 9 | 2 | 0 | Man-9 |
| | | GNN[120]ISLTCIATGR (1375.688) | – | – | – | – | – | – | – | – | – | – | – | glycosylated [g] |
| | | GNN[120]ISLTCIATGRPE (1601.783) | – | – | – | – | – | – | – | – | – | – | – | glycosylated [g] |
| | | GNN[120]ISLTCIATGRPEPTVTWR (2285.159) | – | – | – | – | – | – | – | – | – | – | – | glycosylated [g] |
| | K | LTFFN[252]VSE (955.465) | 20 | 7, A2 | k-4 (2) | 6885 (A) | 1159.4 | 1086.954 (2) | 1086.951 | 0 | 5 | 2 | 0 | Man-5 |
| | | | | | | − (A) | 1159.4 | 1180.493 (2) | 1180.494 | 1 | 4 | 3 | 0 | CoreF(1305.5) |
| | | | | | k-6 (2) | 6824 (A, B) | 1159.4 | 1201.011 (2) | 1201.007 | 1 | 3 | 4 | 0 | CoreF(1305.4) |
| | | | | | | − (A) | 1159.5 | 1261.520 (2) | 1261.520 | 1 | 5 | 3 | 0 | H, CoreF(1305.3) |
| | | | | | k-7 (2) | 6819 (A, B) | 1159.4 | 1302.551 (2) | 1302.546 | 1 | 3 | 5 | 0 | C, CoreF(1305.3), bisectGN(864.6), BA-2 |
| | | | | | | − (A) | 1159.5 | 1334.551 (2) | 1334.549 | 2 | 5 | 3 | 0 | H, CoreF(1305.3), 512(512.3) |
| | | | | | | − (A, B) | 1159.4 | 1355.062 (2) | 1355.062 | 2 | 4 | 4 | 0 | CoreF(1305.2), 512(512.4) |
| | | | | | | − (A, B) | 1159.5 | 1363.059 (2) | 1363.060 | 1 | 5 | 4 | 0 | H, bisectGN(864.4), CoreF(1305.4) or 512(511.9) |
| | | | | | | − (A) | 1160.4 | 1407.068 (2) | 1407.068 | 1 | 5 | 3 | 1 | H, CoreF(1306.4) |
| | | | | | | − (A) | 1159.8 | 1415.576 (2) | 1415.575 | 2 | 6 | 3 | 0 | H, CoreF(1305.3) |

Table 1: Continued

| protein | peptides: sequence[a,b] | glycopeptides: elution position | Figure | peak no.[c] | scan in Figure 4A[d] | observed peptide-related ion[e] | observed m/z in SIM mode[b] | theoretical m/z[b] | N-glycan: deduced monosaccharide composition dHex | Hex | HexNAc | NA | deduced structure[f] (diagnostic ion) |
|---|---|---|---|---|---|---|---|---|---|---|---|---|---|
| | | | | | – (B) | 1159.4 | 957.728 (3) | 957.728 | 2 | 5 | 4 | 0 | H, CoreF(1305.7), $L^{a/x}$ (350.3, 512.1) |
| | | | | k-8 (2) | 6735 (A, B) | 1159.3 | 1436.093 (2) | 1436.089 | 2 | 5 | 4 | 0 | H, CoreF(1305.4), 512(512.3) |
| | | | | | – (A) | 1159.7 | 1444.089 (2) | 1444.086 | 1 | 6 | 4 | 0 | H, CoreF(1305.4) |
| | | | | | – (B) | 1159.5 | 971.404 (3) | 971.404 | 2 | 4 | 5 | 0 | C, CoreF(1305.4), 512(512.3) |
| | | | | k-9 (2) | 6725 (A, B) | 1159.5 | 1456.605 (2) | 1456.602 | 2 | 4 | 5 | 0 | C, (CoreF(1305.4), 512(512.1)) or $L^{b/y}$ (658.2), bisetGN(864.3) |
| | | | | | – (A) | 1160.6 | 1480.098 (2) | 1480.097 | 2 | 5 | 3 | 1 | H, CoreF(1305.3), $sL^{a/x}$ (454.3, 512.2, 657.1, 803.2) |
| | | | | k-1 | 6590 | 1159.3 | 1006.417 (3) | 1006.414 | 3 | 5 | 4 | 0 | C, CoreF(1305.2), $L^{b/y}$ (658.3) |
| | | | | **k-2** | **6658** | **1159.4** | **1011.747 (3)** | **1011.746** | **2** | **6** | **4** | **0** | **H, CoreF(1305.3), $L^{a/x}$ (350.3, 512.1), bisectGN(865.4) [Figure 7, A1]** |
| | | | | | – (A) | 1159.3 | 1517.117 (2) | 1517.115 | 2 | 6 | 4 | 0 | H, CoreF(1305.3), 512(512.1) |
| | | | | | – (A, B) | 1160.4 | 1019.749 (3) | 1019.749 | 1 | 4 | 5 | 1 | C, CoreF(1305.4) |
| | | | | | – (A) | 1159.5 | 1054.760 (3) | 1054.760 | 2 | 5 | 4 | 1 | H, CoreF(1305.5), 512(512.2) |
| | | | | k-3 | 6533 | 1159.5 | 1074.108 (3) | 1074.107 | 3 | 5 | 5 | 0 | C, CoreF(1305.4), $L^{b/y}$ (658.1) |
| | | | | | – (A) | 1159.4 | 1087.442 (3) | 1087.443 | 1 | 4 | 6 | 1 | C, CoreF(1305.4) |
| | | | | | – (A) | 1159.5 | 1122.453 (3) | 1122.453 | 2 | 5 | 5 | 1 | C, CoreF(1305.5), 512(512.2) |
| | | | | k-5 | 6782 (A, B) | 1159.4 | 1190.151 (3) | 1190.146 | 2 | 5 | 6 | 1 | C, CoreF(1305.3), $sL^{a/x}$ (350.2, 512.2, 657.1, 803.2) |
| L | YGN[260]YTCVASNK (1275.555) | 5 | 7, B2 | **l-1** | **2954 (A, B, C)** | **1480.6** | **1078.100 (3)** | **1078.100** | **2** | **4** | **5** | **0** | **C, CoreF(1626.6), bisectGN(1024.9), $L^{a/x}$ (350.3, 512.1) [Figure 7, B1]** |
| | | | | l-1 (2) | 2960 (A) | 1479.5 | 1616.649 (2) | 1616.647 | 2 | 4 | 5 | 0 | C, CoreF(1626.6), bisectGN(1024.4), 512(512.2) |
| | | | | l-2 | 2918 (A) | 1479.6 | 1113.114 (3) | 1113.111 | 3 | 5 | 4 | 0 | H, CoreF(1625.5), $L^{b/y}$ (658.1) |
| | | | | | – (A) | 1480.6 | 1126.446 (3) | 1126.446 | 1 | 4 | 5 | 1 | C, CoreF(1626.6) |
| | | | | l-3 | 3093 | 1478.0 | 1161.457 (3) | 1161.457 | 2 | 5 | 4 | 1 | H, CoreF(1626.7), $sL^{a/x}$ (350.4, 512.1, 657.2, 803.1) |
| | | | | l-4 | 2905 (A, B) | 1479.6 | 1180.806 (3) | 1180.804 | 3 | 5 | 5 | 0 | C, CoreF(1625.6), bisectGN(1024.6), $L^{a/x}$ (350.0, 512.3) |
| | HDYGN[260]YTCVASNK (1527.641) | 8 | – | | 3254 (A, C) | 1732.4 | 1059.426 (3) | 1059.425 | 1 | 3 | 5 | 0 | C, CoreF(1878.7), bisectGN(1150.6), BA-2 |
| | | | | | 3176 (A, C) | 1731.6 | 1162.128 (3) | 1162.129 | 2 | 4 | 5 | 0 | C, (CoreF(1878.7), $L^{a/x}$ (350.1, 512.2)) or $L^{b/y}$ (658.4), bisectGN(1223.8) |

Table 1: Continued

| protein | peptides | | glycopeptides | | | | | | | *N*-glycan | | | | |
|---|---|---|---|---|---|---|---|---|---|---|---|---|---|---|
| | | | | | | | | | | deduced monosaccharide composition | | | | |
| | | sequence[a,b] | elution position | Figure | peak no.[c] | scan in Figure 4A[d] | observed peptide-related ion[e] | observed *m/z* in SIM mode[b] | theoretical *m/z*[b] | dHex | Hex | HexNAc | NA | deduced structure[f] (diagnostic ion) |
| | | | | | | – (C) | 1732.7 | 1197.144 (3) | 1197.139 | 3 | 5 | 4 | 0 | H, CoreF(1877.7), $L^{b/y}$ (512.2, 658.2), bisectiGN(1149.1) |
| | | | | | | 3439 | 1731.7 | 1210.475 (3) | 1210.475 | 1 | 4 | 5 | 1 | C, CoreF(1877.8), bisectGN(1222.6) |
| | | | | | | 3383 | 1732.8 | 1245.488 (3) | 1245.485 | 2 | 5 | 4 | 1 | H, CoreF(1879.7), $sL^{a/x}$ (453.9, 512.2, 657.2, 803.3) |
| | | | | | | 3080 (C) | 1732.7 | 1264.834 (3) | 1264.833 | 3 | 5 | 5 | 0 | C, CoreF(1878.7), bisectGN(1223.4), 512(512.1) |
| | | | | | | 3553 | 1731.9 | 1293.835 (3) | 1293.831 | 1 | 5 | 4 | 2 | H, CoreF(1877.6), bisectGN(1150.5) |
| | | | | | | 3560 | 1731.9 | 1294.175 (3) | 1294.171 | 3 | 5 | 4 | 1 | C, CoreF(1877.7) |
| | M | LGHTN[273]ASIMLFGPGAVSE (1799.888) | 23 | 7, C2 | **m-1** | **7299 (C)** | **1002.6(2)** | **1101.491 (3)** | **1101.488** | **0** | **3** | **5** | **0** | **C, bisectGN(1286.7) [Figure 7, C1]** |
| | | | | | | – (C) | 1003.1(2) | 1141.835 (3) | 1141.830 | 0 | 5 | 4 | 0 | H, bisectGN(1286.5) |
| | | | | | m-2 | 7227 (C) | 1002.6(2) | 1150.176 (3) | 1150.174 | 1 | 3 | 5 | 0 | C, CoreF(1075.6), bisectGN(1357.6), BA-2 |
| | | | | | m-3 | 7210 | 1002.7(2) | 1190.520 (3) | 1190.516 | 1 | 5 | 4 | 0 | H, CoreF(1075.4) or 512(512.0), bisectGN(1359.1) |
| | | | | | m-4 | 7186 | 1002.8(2) | 1244.537 (3) | 1244.534 | 1 | 6 | 4 | 0 | H, 512(512.2) |
| Kilon | N | GAWLN[36]R (715.377) | 3 | 8, A2 | | – (B) | 919.5 | 966.907 (2) | 966.907 | 0 | 5 | 2 | 0 | Man-5 |
| | | | | | **n-1 (2)** | **2664 (A, B, C)** | **919.5** | **1047.934 (2)** | **1047.933** | **0** | **6** | **2** | **0** | **Man-6 [Figure 8, A1]** |
| | | | | | n-2 (2) | 2706 (A, B, C) | 919.5 | 1128.960 (2) | 1128.960 | 0 | 7 | 2 | 0 | Man-7 |
| | | | | | n-3 (2) | 2679 (A, B, C) | 919.4 | 1209.988 (2) | 1209.986 | 0 | 8 | 2 | 0 | Man-8 |
| | | CYLEDGASGAWLN[36]R (1738.810) | 18 | – | | 5234 | 972.3 | 1040.101 (3) | 1040.102 | 0 | 6 | 2 | 0 | Man-6 |
| | O | GTN[118]VTLTCLATGKPE (1560.782) | 16 | 8, B2 | **o-1** | **4760** | **1765.8** | **1070.475 (3)** | **1070.472** | **1** | **3** | **5** | **0** | **C, CoreF(1910.8), bisectGN(1167.3), BA-2 [Figure 8, B1]** |
| | | | | | o-2 | 4683 | 1764.7 | 1105.485 (3) | 1105.483 | 2 | 4 | 4 | 0 | CoreF(1910.9), bisectGN(1167.8), 512(512.2) |
| | | | | | o-3 | 4710 (C) | 1765.7 | 1173.176 (3) | 1173.176 | 2 | 4 | 5 | 0 | C, CoreF(1911.9), bisectGN(1167.3), 512(512.1) |
| | | | | | o-4 | 4638 | 1765.8 | 1275.880 (3) | 1275.879 | 3 | 5 | 5 | 0 | C, CoreF(1910.9), 512(512.1) |
| | | | | | o-5 | 4857 (C) | 1765.0 | 1324.227 (3) | 1324.225 | 2 | 5 | 5 | 1 | C, CoreF(1910.8), 512(512.1) |
| | | | | | | – (C) | 1764.9 | 1401.911 (3) | 1401.910 | 1 | 5 | 4 | 3 | C, CoreF(1911.0) |
| | P | LFNGQQGIIIQN[238]FSTR (1834.969) | 22 | 8, C2 | **p-1** | **7203 (C)** | **1020.3(2)** | **1018.138 (3)** | **1018.138** | **0** | **5** | **2** | **0** | **Man-5 [Figure 8, C1]** |
| | | RLFNGQQGIIIQN[238]FSTR (1991.070) | 21 | – | | 6895 (C) | 1098.3(2) | 1070.171 (3) | 1070.172 | 0 | 5 | 2 | 0 | Man-5 |
| | | KRLFNGQQGIIIQN[238]FSTR (2119.165) | 19 | – | | 6165 (C) | 1162.4(2) | 1112.871 (3) | 1112.870 | 0 | 5 | 2 | 0 | Man-5 |
| | Q | SILTVTN[249]VTQE (1203.635) | 17 | 8, D2 | q-8 (2) | 5086 (A, C) | 1407.5 | 1211.037 (2) | 1211.036 | 0 | 5 | 2 | 0 | Man-5 |
| | | | | | | – (B) | 1407.7 | 883.729 (3) | 883.730 | 1 | 3 | 4 | 0 | CoreF(1553.5), bisectGN(1061.5) |

Table 1: Continued

| peptides | | | glycopeptides | | | | | | *N*-glycan | | | | |
|---|---|---|---|---|---|---|---|---|---|---|---|---|---|
| | | | | | | | | | deduced monosaccharide composition | | | | |
| protein | sequence[a,b] | elution position | Figure | peak no.[c] | scan in Figure 4A[d] | observed peptide-related ion[e] | observed *m/z* in SIM mode[b] | theoretical *m/z*[b] | dHex | Hex | HexNAc | NA | deduced structure[f] (diagnostic ion) |
| | | | | q-10 (2) | 5059 (A, C) | 1407.4 | 1325.094 (2) | 1325.092 | 1 | 3 | 4 | 0 | CoreF(1553.5) or 512(512.2), bisectGN(988.6) |
| | | | | | – (B) | 1407.6 | 951.423 (3) | 951.423 | 1 | 3 | 5 | 0 | C, CoreF(1553.6), bisectGN(988.6), BA-2 |
| | | | | | – (A) | 1407.6 | 1426.632 (2) | 1426.631 | 1 | 3 | 5 | 0 | C, CoreF(1553.5), bisectGN(988.2), BA-2 |
| | | | | q-11 (2) | 4950 (A, C) | 1407.5 | 1458.635 (2) | 1458.634 | 2 | 5 | 3 | 0 | H, CoreF(1553.4), 512(512.2) |
| | | | | | – (B) | 1407.3 | 991.765 (3) | 991.765 | 1 | 5 | 4 | 0 | H, CoreF(1553.6) |
| | | | | | – (A) | 1407.6 | 1487.143 (2) | 1487.144 | 1 | 5 | 4 | 0 | H, CoreF(1553.4) |
| | | | | q-1 | 5126 (A) | 1407.5 | 1021.106 (3) | 1021.104 | 1 | 5 | 3 | 1 | H, CoreF(1553.4) or 512(512.2) |
| | | | | | – (A) | 1407.6 | 1531.153 (2) | 1531.152 | 1 | 5 | 3 | 1 | H, CoreF(1553.6) or 512(512.0) |
| | | | | q-2 | 4885 (C) | 1407.4 | 1026.777 (3) | 1026.776 | 2 | 6 | 3 | 0 | H, CoreF(1553.5), $L^{a/x}$ (350.3, 512.2) |
| | | | | q-2 (2) | 4919 (C) | 1407.6 | 1539.663 (2) | 1539.660 | 2 | 6 | 3 | 0 | H, CoreF(1554.2), 512(512.1) |
| | | | | q-3 | 5010 (A, C) | 1407.5 | 1040.453 (3) | 1040.451 | 2 | 5 | 4 | 0 | H, CoreF(1553.6), $L^{a/x}$ (350.2, 512.1) |
| | | | | | – (A) | 1407.5 | 1560.174 (2) | 1560.173 | 2 | 5 | 4 | 0 | H, CoreF(1553.4), 512(512.2) |
| | | | | **q-4** | **4944 (A, C)** | **1406.6** | **1054.128 (3)** | **1054.127** | **2** | **4** | **5** | **0** | **C, CoreF(1552.6)s, $L^{a/x}$ (350.2, 512.1) [Figure 8, D1]** |
| | | | | | – (A) | 1407.6 | 1580.687 (2) | 1580.687 | 2 | 4 | 5 | 0 | C, CoreF(1553.6), 512(512.2) |
| | | | | | – (A) | 1407.5 | 1075.121(3) | 1075.122 | 1 | 6 | 3 | 1 | H, CoreF(1554.6) |
| | | | | | – (A) | 1407.6 | 1612.180 (2) | 1612.179 | 1 | 6 | 3 | 1 | H, CoreF(1554.5) |
| | | | | q-5 | 4827 | 1407.5 | 1089.139 (3) | 1089.137 | 3 | 5 | 4 | 0 | H, CoreF(1553.6), 512(512.1) |
| | | | | | – (A) | 1407.5 | 1094.469 (3) | 1094.469 | 2 | 6 | 4 | 0 | H, CoreF(1554.3), $L^{a/x}$ (350.3, 512.2) |
| | | | | | – (A) | 1407.3 | 1102.473 (3) | 1102.473 | 1 | 4 | 5 | 1 | C, CoreF(1552.7) |
| | | | | q-6 | 5032 | 1407.5 | 1137.486 (3) | 1137.483 | 2 | 5 | 4 | 1 | C, CoreF(1553.3), 512(512.2) |
| | | | | q-7 | 4869 (A) | 1407.6 | 1156.832 (3) | 1156.830 | 3 | 5 | 5 | 0 | C, CoreF(1553.5) |
| | | | | | – (A) | 1407.6 | 1170.166 (3) | 1170.166 | 1 | 4 | 6 | 1 | C, CoreF(1553.3) or ($sL^{a/x}$ (512.4, 803.6) |
| | | | | q-9 | 5054 (A) | 1407.4 | 1272.870 (3) | 1272.869 | 2 | 5 | 6 | 1 | C, CoreF(1553.5) ($sL^{a/x}$ (454.1, 512.2, 657.2, 803.2)) |
| R | HFGN[257]YTCVAANK (1380.624) | 10 | 8, E2 | | – (B) | 793.2(2) | 866.690 (3) | 866.690 | 0 | 5 | 2 | 0 | Man-5 |
| | | | | r-7 (2) | 3214 (C) | 1584.7 | 1299.536 (2) | 1299.531 | 0 | 5 | 2 | 0 | Man-5 |
| | | | | r-1 | 3339 (C) | 1584.6 | 1010.422 (3) | 1010.420 | 1 | 3 | 5 | 0 | C, CoreF(1730.6), bisectGN(1077.0), BA-2 |
| | | | | **r-2** | **3162 (A, C)** | **1584.7** | **1050.764 (3)** | **1050.762** | **1** | **5** | **4** | **0** | **H, CoreF(1730.5), bisectGN(1077.7) [Figure 8, E1]** |
| | | | | r-3 | 3139 (A, C) | 1585.9 | 1085.774 (3) | 1085.772 | 2 | 6 | 3 | 0 | H, CoreF(1730.8), $L^{a/x}$ (350.2, 512.2) |